

# Systematic shell-model study of $^{98-130}\text{Cd}$ isotopes

Deepak Patel and Praveen C. Srivastava\*<sup>1</sup>

<sup>1</sup>*Department of Physics, Indian Institute of Technology Roorkee, Roorkee 247667, India*

(Dated: February 16, 2023)

We have performed shell-model calculations for the systematic study of even-even  $^{98-130}\text{Cd}$  isotopes with  $\Delta\text{NNLO}_{\text{GO}}$  interaction derived from coupled cluster approach, where  $^{84}\text{Se}$  is taken as an inert core. Results for these Cd-isotopes using a realistic effective shell-model interaction, derived from the G-matrix approach with core  $^{88}\text{Sr}$ , have also been shown. We have compared our calculated low-lying excited energy spectra and electromagnetic properties with the experimental data. On the basis of recently available experimental data, we have also predicted spins and parities corresponding to unconfirmed states. We have also reported the properties of  $8^+$  isomeric states in  $^{98-104,130}\text{Cd}$  isotopes.

PACS numbers: 21.60.Cs, 23.20.-g, 23.20.Lv, 27.60.+j

## I. INTRODUCTION

In recent years, the study of nuclear structure properties of Cd and Te isotopes has increased both from the experimental and theoretical sides because they are in the vicinity of the  $^{100}\text{Sn}$ , which is the heaviest  $N = Z$  doubly magic nucleus [1–5]. The study of nuclear properties in Cd isotopes is also essential for the understanding of stellar nucleosynthesis. Several similarities are pointed out between Sn and Cd isotopic chains, like excitation energy spectra and electric quadrupole transition probability [3, 6–12]. The shell-model provides a better platform to verify these properties.

In the past, the energy states in Cd-isotopes have been measured using different advanced experimental techniques. Górska *et al.* [13] studied the  $\gamma$ -decay and  $8^+$  isomer in  $^{100}\text{Cd}$  using a recoil catcher setup inside the multidetector  $\gamma$ -array OSIRIS. For the first time, Alber *et al.* [14] experimentally observed the low-lying spectra of neutron-deficient  $^{100-102}\text{Cd}$ . Measurements of lifetimes of excited nuclear states are important for computing  $B(E2)$  transition rates. Lieb *et al.* [15] determined picosecond lifetimes of high-spin states in  $^{102}\text{Cd}$  isotope using the reaction  $^{58}\text{Ni}(^{50}\text{Cr}, \alpha 2p)$  and coincidence recoil distance Doppler-shift technique (RDDS). Boelaert *et al.* [16] determined the lifetimes of low-lying  $2_1^+$  and  $4_1^+$  states in  $^{104}\text{Cd}$  and  $2_1^+$  state in  $^{102}\text{Cd}$ . Müller *et al.* [17] determined lifetimes of high-spin states in  $^{104}\text{Cd}$  in the time range  $0.3 \text{ ps} \leq \tau \leq 1.2 \text{ ns}$  for the first time using RDDS and Doppler-shift attenuation methods (DSAM). They have also discussed new experimental results in  $^{104}\text{Cd}$  in the frame of the interacting boson plus broken pair model. Simons *et al.* [18] measured the lifetimes of excited states in the lowest-lying positive parity bands in  $^{106,108}\text{Cd}$  isotopes using the RDDS and also deduced the  $B(E2)$  transition rates. Benczer-Koller *et al.* [19] remeasured and supplemented existing lifetimes and magnetic moments of low-lying states in  $^{106}\text{Cd}$ . Fan *et al.* [20] measured g-factors of rotational states of the yrast band from spin  $10^+$  to spin  $16^+$  in  $^{108}\text{Cd}$  using transient-magnetic-field ion implantation perturbed angular distribution method. Kumpulainen *et al.* [21] investigated the low-lying low-spin collective states in even  $^{106-112,116}\text{Cd}$  isotopes using in-beam and off-beam  $\gamma$ -ray and conversion-electron spectroscopy. Gade *et al.* [22] reported the first evidence for the complete quadrupole-octupole coupled quintuplet of negative parity  $(2_1^- \otimes 3_1^-)^{(J^-)}$  with  $J = 1, 2, 3, 4, 5$  for  $^{108}\text{Cd}$ . Nomura *et al.* [23] investigated the structure of even-even  $^{108-116}\text{Cd}$  isotopes using a self-consistent mean-field approach. Corminboeuf *et al.* [24] performed measurements consisting of  $\gamma$ -ray excitation functions and angular distributions on  $^{110}\text{Cd}$ . They extracted the lifetimes for 16 excited states using the DSAM. Piiparinen *et al.* [25] measured lifetimes of 20 yrast levels in  $^{110}\text{Cd}$  using the recoil-distance method and the NORDBALL array of Compton-suppressed Ge-detectors. They also deduced the reduced-transition probabilities and revealed the rotational and vibrational behavior of  $^{110}\text{Cd}$ . After that, Regan *et al.* [26] measured the gyromagnetic ratio of yrast  $10^+$  state in  $^{110}\text{Cd}$  using ion-implantation perturbed-angular-distribution (IMPAD) technique. Garrett *et al.* [27] measured lifetimes of those levels which are below 4 MeV in  $^{112}\text{Cd}$  isotope using DSAM following the inelastic scattering of monoenergetic neutrons. Jamieson *et al.* [28] studied the quadrupole-octupole coupled states in  $^{112}\text{Cd}$  with  $^{111}\text{Cd}(d, p)^{112}\text{Cd}$  reaction using 22 MeV polarized deuterons. Zamfir *et al.* [29] studied the structure of  $^{122}\text{Cd}$  through the decay of  $^{122}\text{Ag}$  by  $\gamma - \gamma$  coincidences,  $\gamma$ -ray angular correlations, and  $\beta - \gamma - \gamma$  fast electronic scintillation timing (FEST) measurements. Scherillo *et al.* [30] investigated microsecond isomers in Cd isotopes in the mass range  $A=123$  to 130 using the LOHENGRIN mass spectrometer. Hoteling *et al.* [31] identified

\* Corresponding author: praveen.srivastava@ph.iitr.ac.in

the presence of isomeric levels with half-lives in the microsecond range in  $^{125-128}\text{Cd}$ . In a recent TITAN experiment at TRIUMF, the cadmium masses were measured for  $^{125/m}\text{Cd}$  and  $^{126}\text{Cd}$ . Lascar *et al.* [32] presented the results of precision mass measurements of  $^{125-127}\text{Cd}$  isotopes. They have also compared their measurements with the *ab initio* shell-model calculations. Dunlop *et al.* [33] measured the  $\beta$ -decay half-lives of  $^{128-130}\text{Cd}$  isotopes using GRIFFIN  $\gamma$ -ray spectrometer at the TRIUMF-ISAC facility. Dillmann *et al.* [34] performed the first  $\beta$ - and  $\gamma$ -spectroscopic decay of the  $N = 82$  r-process “waiting-point” nuclide  $^{130}\text{Cd}$  at CERN-ISOLDE.

In the previous theoretical works, Schmidt *et al.* [35] performed shell-model calculations for even-even  $^{98-108}\text{Cd}$  isotopes. Blazhev *et al.* [36] identified a core excited  $I^\pi=(12^+)$  spin-gap isomer in  $^{98}\text{Cd}$ . They have also discussed the measured  $E4$  and  $E2$  strengths,  $^{100}\text{Sn}$  core excitations, and the origin of empirical polarization charges in large-scale shell-model calculations. Boelaert *et al.* [37] performed shell-model calculations for even-even  $^{98-106}\text{Cd}$  isotopes and calculated energy spectra and transition probabilities. Clark *et al.* [38] studied the gamma decay of excited states in  $^{100}\text{Cd}$  with Gammasphere array following the  $^{46}\text{Ti}(^{58}\text{Ni},2p,2n)$  reaction at 215 MeV. They compared their results with shell-model calculations. Maheshwari *et al.* [39] studied the energy variation of  $2_1^+$  states and  $B(E2;0_1^+ \rightarrow 2_1^+)$  trends in the Cd, Sn and Te isotopic chains using generalized seniority approach.

The aim of the present paper is to perform systematic shell-model calculations for even  $^{98-130}\text{Cd}$  isotopes. We have investigated different properties of these isotopes like excitation energy, reduced electromagnetic transition probabilities, isomeric states, electric quadrupole, and magnetic moments from neutron-deficient isotopes (near the proton drip line) to the neutron-rich isotopes up to  $N = 82$ . Recently, several new experimental data are available in Cd isotopic chain for low-lying spin states. Therefore, we have focused here on the low-lying spin states of these isotopes.

This paper is divided into the following sections. In Section II, the formalism for coupled cluster method and the resulting similarity transformed Hamiltonian is briefly discussed. In Section III, we introduce the monopole shifts in the single-particle energies of valence proton orbitals for Cd-isotopes. In Section IV, we present our calculated results of low-lying energy spectra, electromagnetic properties, octupole collective  $3^-$  states, and  $8^+$  isomeric states in the Cd chain. Finally, we summarize our results and conclude the paper in section V.

## II. FORMALISM

The nuclear shell-model Hamiltonian can be expressed in terms of single-particle energies and two nucleon interactions,

$$H = \sum_{\alpha} \epsilon_{\alpha} c_{\alpha}^{\dagger} c_{\alpha} + \frac{1}{4} \sum_{\alpha\beta\gamma\delta JT} \langle j_{\alpha} j_{\beta} | V | j_{\gamma} j_{\delta} \rangle_{JT} c_{\alpha}^{\dagger} c_{\beta}^{\dagger} c_{\delta} c_{\gamma} \quad (1)$$

where  $\alpha = \{n, l, j, t\}$  stand for the single-particle orbitals and  $\epsilon_{\alpha}$  are corresponding single-particle energies.  $c_{\alpha}$  and  $c_{\alpha}^{\dagger}$  are the fermion annihilation and creation operators.  $\langle j_{\alpha} j_{\beta} | V | j_{\gamma} j_{\delta} \rangle_{JT}$  denote the antisymmetrized two-body matrix elements coupled to spin  $J$  and isospin  $T$ .

We have studied the structure of even-even Cd isotopes from the neutron numbers 50 to 82 using two types of interactions and model spaces. The first effective interaction is derived through the shell-model coupled cluster (SMCC) approach based on similarity transformations. In the medium-mass nuclei, the coupled cluster method is useful for *ab initio* calculations. Here, we have taken a chiral interaction named  $\Delta\text{NNLO}_{\text{GO}}$  [40] interaction. We have mainly focused on the application of this interaction in the even-even  $^{98-130}\text{Cd}$  chain. The shell model code KSHELL [41] has been used for our calculations to diagonalize the matrices. The highest dimension is  $1.77 \times 10^9$  for  $^{114}\text{Cd}$  with  $\Delta\text{NNLO}_{\text{GO}}$  interaction. For the interaction  $\Delta\text{NNLO}_{\text{GO}}$ , the model space consist of  $1p_{3/2}$ ,  $1p_{1/2}$ ,  $0g_{9/2}$  proton orbitals and  $1d_{5/2}$ ,  $2s_{1/2}$ ,  $1d_{3/2}$ ,  $0g_{7/2}$ ,  $0h_{11/2}$  neutron orbitals with core  $^{84}\text{Se}$ . We have performed our calculations with this interaction without any truncation. The formalism to find an effective Hamiltonian is given below.

The intrinsic Hamiltonian for coupled-cluster calculations [42] can be written as-

$$H = \left(1 - \frac{1}{A}\right) \sum_{i=1}^A \frac{p_i^2}{2m} + \sum_{i<j=1}^A \left\{ V_{ij} - \frac{\vec{p}_i \cdot \vec{p}_j}{mA} \right\} + \sum_{i<j<k}^A V_{ijk} \quad (2)$$

Here,  $A$  is the mass number,  $m$  is the mass of a nucleon,  $p_i$  and  $p_j$  are single-particle momentum,  $V_{ij}$  is the nucleon-nucleon interaction, and  $V_{ijk}$  is the three-body interaction.

The normal-ordered Hamiltonian for shell-model coupled-cluster (SMCC) calculations with respect to a Hartree-Fock reference state  $|\phi_0\rangle$  can be expressed as-

$$\mathcal{H} = E_0 + \sum_{ab} g_{ab} \{a^\dagger b\} + \frac{1}{4} \sum_{abcd} V_{abcd} \{a^\dagger b^\dagger dc\} + \frac{1}{36} \sum_{abcdef} V_{abc,def} \{a^\dagger b^\dagger c^\dagger def\}. \quad (3)$$

$a^\dagger$  is particle creation operator and  $a$  is particle annihilation operator on state  $|\phi_a\rangle$ .  $g_{ab}$  denote the Fock-matrix elements, while  $V_{abcd}$  and  $V_{abc,def}$  denote the two-body and three-body matrix elements, respectively. For our calculations, the Hamiltonian given by equation (3) is truncated at the two-body level. The energy expectation value of the reference state is given by  $E_0 = \langle \phi_0 | H | \phi_0 \rangle$  where  $H$  is the intrinsic Hamiltonian.

The wave function of the coupled-cluster theory can be written as an exponential ansatz,

$$|\phi\rangle = e^T |\phi_0\rangle \quad (4)$$

where  $T$  is the cluster operator.

The similarity-transformed Hamiltonian [42] is given by,  $\overline{\mathcal{H}} \equiv e^{-T} \mathcal{H} e^T$ , can be expanded as-

$$\overline{\mathcal{H}} = E_{CC} + \sum_{ab} \overline{\mathcal{H}}_{ab} \{a^\dagger b\} + \sum_{abcd} \overline{\mathcal{H}}_{abcd} \{a^\dagger b^\dagger dc\} + \sum_{abcdef} \overline{\mathcal{H}}_{abcdef} \{a^\dagger b^\dagger c^\dagger fed\} + \dots, \quad (5)$$

Here,  $E_{CC} = \langle \phi_0 | \overline{\mathcal{H}} | \phi_0 \rangle$  is the correlation energy.

To construct a shell-model effective interaction, we split infinite Hilbert space into the model space  $P$  and its complement  $Q$ . Which obey the relation-

$$P + Q = 1 \quad (6)$$

To decouple the  $P$  space from  $Q$  space for the Hamiltonian, a secondary similarity transformation is applied to the coupled-cluster Hamiltonian,

$$\overline{\overline{\mathcal{H}}} = e^{-S} \overline{\mathcal{H}} e^S \quad (7)$$

Where  $S$  is an  $A$ -body operator.

The decoupling between  $P$  and  $Q$  space requires,

$$Q \overline{\overline{\mathcal{H}}} P = 0 \quad (8)$$

which results the effective Hamiltonian,

$$H_{eff} = P \overline{\overline{\mathcal{H}}} P. \quad (9)$$

More details about effective interaction is given in Ref. [42].

We have also performed shell-model calculations with the G-matrix effective interaction [37], which is constructed by the effective microscopic interaction derived from a charge-symmetry breaking nucleon-nucleon potential [43] and another interaction from [44] (named v3rd), with further modifications in the monopole part. This interaction consist of  $1p_{1/2}$ ,  $0g_{9/2}$  proton orbitals and  $1d_{5/2}$ ,  $2s_{1/2}$ ,  $1d_{3/2}$ ,  $0g_{7/2}$ ,  $0h_{11/2}$  neutron orbitals with core  $^{88}\text{Sr}$ .

### III. MONOPOLE SHIFT

In the case of  $^{98-130}\text{Cd}$ , there are two valence proton holes and several valence neutrons outside the doubly magic nucleus  $^{100}\text{Sn}$ . It can be expected that the proton-neutron interaction will influence the effective single-particle energies of the proton orbitals. The effective single-particle energies depend on the proton-neutron effective interactions and the pairing properties between the neutron [45]. The variation in the single-particle energy of valence proton orbital as a function of neutron number is known as the monopole shift [46]. The low-lying states carry a significant part of the proton single-particle strength for these isotopes. In Cd isotopes, valence protons in  $j_\pi$  orbitals interact with a

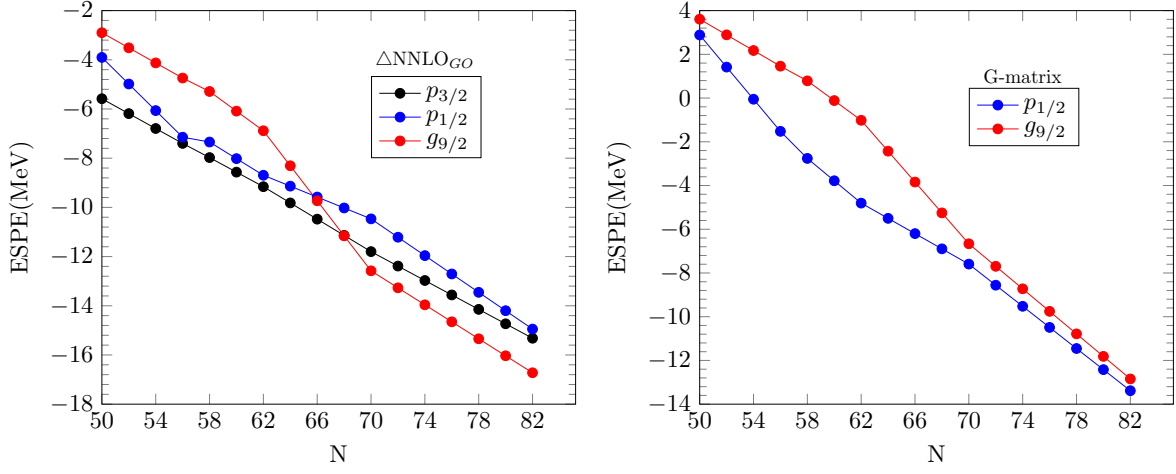


FIG. 1: Variation in the effective single particle energies in Cd isotopes corresponding to  $\Delta\text{NNLO}_{\text{GO}}$ , and the G-matrix interactions.

number of valence protons and neutrons in proton orbitals  $j_\pi$  and neutron orbitals  $j_\nu$ , respectively. The Hamiltonian can be written as

$$\hat{H} = \epsilon_{j_\pi} + \sum_{j_\nu} \epsilon_{j_\nu} \hat{n}_{j_\nu} + V_{\pi\pi} + V_{\pi\nu} + V_{\nu\nu} \quad (10)$$

Here  $\epsilon_{j_\pi}$  and  $\epsilon_{j_\nu}$  are single-particle energies of proton and neutron corresponding to  $j_\pi$  and  $j_\nu$  orbitals, respectively.  $\hat{n}_{j_\nu}$  is the number operator for neutrons.  $V_{\pi\pi}$ ,  $V_{\pi\nu}$  and  $V_{\nu\nu}$  represent residual proton-proton, proton-neutron, and neutron-neutron interactions, respectively.

For different multipole components of these interactions,  $\hat{H}$  can be written as

$$\hat{H} = \hat{H}_{\lambda=0} + \hat{H}_{\lambda=1} + \dots + \text{higher } \lambda \text{ multipoles of } \pi\pi, \pi\nu \text{ and } \nu\nu \text{ interaction.} \quad (11)$$

We can write the monopole Hamiltonian  $\hat{H}_{\lambda=0}$  as

$$\hat{H}_{\lambda=0} = \sum_{j_\pi} \tilde{\epsilon}_{j_\pi} \hat{n}_{j_\pi} + \sum_{j_\nu} \tilde{\epsilon}_{j_\nu} \hat{n}_{j_\nu}. \quad (12)$$

Here  $\tilde{\epsilon}_{j_\pi}$  is the effective proton single-particle energy, which is given as

$$\tilde{\epsilon}_{j_\pi} = \epsilon_{j_\pi} + \sum_{j_\pi} \bar{E}(j_\pi j_\pi) \hat{n}_{j_\pi} + \sum_{j_\nu} \bar{E}(j_\pi j_\nu) \hat{n}_{j_\nu}. \quad (13)$$

Where  $\bar{E}(j_\pi j_\pi)$  and  $\bar{E}(j_\pi j_\nu)$  are monopole matrix elements [47]. They can be expressed as

$$\bar{E}(j_\pi j_\pi) = \frac{\sum_J (2J+1) \langle j_\pi j_\pi; J | V | j_\pi j_\pi; J \rangle}{\sum_J (2J+1)} \quad (14)$$

and

$$\bar{E}(j_\pi j_\nu) = \frac{\sum_J (2J+1) \langle j_\pi j_\nu; J | V | j_\pi j_\nu; J \rangle}{\sum_J (2J+1)} \quad (15)$$

In Fig. 1, we have shown the change in effective single-particle energy (ESPE) of proton orbitals with respect to neutron number in Cd-isotopes for  $\Delta\text{NNLO}_{\text{GO}}$ , and the G-matrix interactions. We can see that the variation in effective single particle energy of the proton orbitals is different from neutron-deficient to neutron-rich side.

TABLE I: The calculated shell model wave functions corresponding to  $2_1^+$  state in even-even  $^{98-130}\text{Cd}$  isotopes.

Nuclei	State	Probability	$\Delta\text{NNLO}_{\text{GO}}$	Probability	G-matrix
$^{98}\text{Cd}$	$2_1^+$	98.8%	$\pi(p_{3/2}^4 p_{1/2}^2 g_{9/2}^8)$	100%	$\pi(p_{1/2}^2 g_{9/2}^8)$
$^{100}\text{Cd}$	$2_1^+$	52.2%	$\pi(p_{3/2}^4 p_{1/2}^2 g_{9/2}^8) \otimes \nu(g_{7/2}^2)$	55.9%	$\pi(p_{1/2}^2 g_{9/2}^8) \otimes \nu(d_{5/2}^2)$
$^{102}\text{Cd}$	$2_1^+$	36.3%	$\pi(p_{3/2}^4 p_{1/2}^2 g_{9/2}^8) \otimes \nu(g_{7/2}^2 d_{5/2}^2)$	27.8%	$\pi(p_{1/2}^2 g_{9/2}^8) \otimes \nu(d_{5/2}^4)$
$^{104}\text{Cd}$	$2_1^+$	25.1%	$\pi(p_{3/2}^4 p_{1/2}^2 g_{9/2}^8) \otimes \nu(g_{7/2}^4 d_{5/2}^2)$	32.1%	$\pi(p_{1/2}^2 g_{9/2}^8) \otimes \nu(d_{5/2}^4 g_{7/2}^2)$
$^{106}\text{Cd}$	$2_1^+$	21.5%	$\pi(p_{3/2}^4 p_{1/2}^2 g_{9/2}^8) \otimes \nu(g_{7/2}^4 d_{5/2}^4)$	26.5%	$\pi(p_{1/2}^2 g_{9/2}^8) \otimes \nu(d_{5/2}^4 g_{7/2}^4)$
$^{108}\text{Cd}$	$2_1^+$	13.6%	$\pi(p_{3/2}^4 p_{1/2}^2 g_{9/2}^8) \otimes \nu(g_{7/2}^6 d_{5/2}^4)$	10.8%	$\pi(p_{1/2}^2 g_{9/2}^8) \otimes \nu(d_{5/2}^4 g_{7/2}^6)$
$^{110}\text{Cd}$	$2_1^+$	9.6%	$\pi(p_{3/2}^4 p_{1/2}^2 g_{9/2}^8) \otimes \nu(g_{7/2}^6 d_{5/2}^6)$	6.8%	$\pi(p_{1/2}^2 g_{9/2}^8) \otimes \nu(d_{5/2}^4 g_{7/2}^6 h_{11/2}^2)$
$^{112}\text{Cd}$	$2_1^+$	4.0%	$\pi(p_{3/2}^4 p_{1/2}^2 g_{9/2}^8) \otimes \nu(g_{7/2}^6 d_{5/2}^6 h_{11/2}^2)$	8.5%	$\pi(p_{1/2}^2 g_{9/2}^8) \otimes \nu(d_{5/2}^6 g_{7/2}^4 d_{3/2}^2 h_{11/2}^2)$
$^{114}\text{Cd}$	$2_1^+$	3.2%	$\pi(p_{3/2}^3 p_{1/2}^1 g_{9/2}^{10}) \otimes \nu(g_{7/2}^8 d_{5/2}^6 h_{11/2}^2)$	8.2%	$\pi(p_{1/2}^2 g_{9/2}^8) \otimes \nu(d_{5/2}^4 g_{7/2}^6 d_{3/2}^2 h_{11/2}^4)$
$^{116}\text{Cd}$	$2_1^+$	3.0%	$\pi(p_{3/2}^3 p_{1/2}^1 g_{9/2}^{10}) \otimes \nu(g_{7/2}^8 d_{5/2}^6 h_{11/2}^4)$	11.3%	$\pi(p_{1/2}^2 g_{9/2}^8) \otimes \nu(d_{5/2}^6 g_{7/2}^6 d_{3/2}^2 h_{11/2}^4)$
$^{118}\text{Cd}$	$2_1^+$	2.6%	$\pi(p_{3/2}^3 p_{1/2}^1 g_{9/2}^{10}) \otimes \nu(g_{7/2}^8 d_{5/2}^6 h_{11/2}^6)$	20.9%	$\pi(p_{1/2}^2 g_{9/2}^8) \otimes \nu(d_{5/2}^6 g_{7/2}^6 d_{3/2}^2 h_{11/2}^6)$
$^{120}\text{Cd}$	$2_1^+$	2.9%	$\pi(p_{3/2}^3 p_{1/2}^1 g_{9/2}^{10}) \otimes \nu(g_{7/2}^8 d_{5/2}^6 d_{3/2}^2 h_{11/2}^6)$	24.3%	$\pi(p_{1/2}^2 g_{9/2}^8) \otimes \nu(d_{5/2}^6 g_{7/2}^6 d_{3/2}^2 h_{11/2}^8)$
$^{122}\text{Cd}$	$2_1^+$	3.7%	$\pi(p_{3/2}^3 p_{1/2}^1 g_{9/2}^{10}) \otimes \nu(g_{7/2}^8 d_{5/2}^6 d_{3/2}^2 h_{11/2}^8)$	35.9%	$\pi(p_{1/2}^2 g_{9/2}^8) \otimes \nu(d_{5/2}^6 s_{1/2}^2 g_{7/2}^6 d_{3/2}^2 h_{11/2}^8)$
$^{124}\text{Cd}$	$2_1^+$	4.8%	$\pi(p_{3/2}^3 p_{1/2}^1 g_{9/2}^{10}) \otimes \nu(g_{7/2}^8 d_{5/2}^6 d_{3/2}^2 h_{11/2}^{10})$	28.2%	$\pi(p_{1/2}^2 g_{9/2}^8) \otimes \nu(d_{5/2}^6 s_{1/2}^2 g_{7/2}^6 d_{3/2}^2 h_{11/2}^{10})$
$^{126}\text{Cd}$	$2_1^+$	6.4%	$\pi(p_{3/2}^3 p_{1/2}^1 g_{9/2}^{10}) \otimes \nu(g_{7/2}^8 d_{5/2}^6 d_{3/2}^2 h_{11/2}^{12})$	43.8%	$\pi(p_{1/2}^2 g_{9/2}^8) \otimes \nu(d_{5/2}^6 s_{1/2}^2 g_{7/2}^8 d_{3/2}^2 h_{11/2}^{10})$
$^{128}\text{Cd}$	$2_1^+$	12.9%	$\pi(p_{3/2}^3 p_{1/2}^1 g_{9/2}^{10}) \otimes \nu(g_{7/2}^8 d_{5/2}^6 d_{3/2}^4 h_{11/2}^{12})$	80.5%	$\pi(p_{1/2}^2 g_{9/2}^8) \otimes \nu(d_{5/2}^6 s_{1/2}^2 g_{7/2}^8 d_{3/2}^4 h_{11/2}^{10})$
$^{130}\text{Cd}$	$2_1^+$	91.1%	$\pi(p_{3/2}^3 p_{1/2}^1 g_{9/2}^{10}) \otimes \nu(g_{7/2}^8 d_{5/2}^6 d_{3/2}^4 s_{1/2}^2 h_{11/2}^{12})$	100%	$\pi(p_{1/2}^2 g_{9/2}^8) \otimes \nu(d_{5/2}^6 s_{1/2}^2 g_{7/2}^8 d_{3/2}^4 h_{11/2}^{12})$

## IV. RESULTS

### A. Low-lying energy spectra of $^{98-130}\text{Cd}$ even isotopes

We have compared the experimental data of energy levels with two interactions named  $\Delta\text{NNLO}_{\text{GO}}$ , and the G-matrix interaction for  $^{98-130}\text{Cd}$  isotopes as shown in Figs. 2-6. We have shown five states maximally for a given spin-parity  $J^\pi$ . The wave function corresponding to  $2_1^+$  state for  $^{98-130}\text{Cd}$  isotopes are shown in Table I.

Górska *et al.* [49] identified and studied excited states in  $^{98}\text{Cd}$  (two proton holes from  $^{100}\text{Sn}$ ) using in-beam spectroscopy for the first time. They also populated states up to  $8^+$  isomer and compared it to the shell-model predictions. In the case of  $^{98}\text{Cd}$ , the G-matrix interaction shows good agreement with the experimental data for the  $2_1^+$  and  $4_1^+$  states. For this interaction, the  $6_1^+$  and  $8_1^+$  states are also comparable with the experimental data but compressed from the  $\Delta\text{NNLO}_{\text{GO}}$  interaction. The energy gap between  $8_1^+$  and  $6_1^+$  is very close with both interactions as in the experimental data. From both interactions, the ground state  $0^+$  and other excited states up to  $8^+$  show  $\pi(g_{9/2}^-)$  character, which corresponds to the single-particle behavior of this isotope. We have also performed shell-model calculations for  $0_2^+$ ,  $5_1^-$  and  $4_1^-$  states as reported in the Ref. [49]. With G-matrix interaction, the location of these states are comparable to the results obtained in Ref. [49]. From  $\Delta\text{NNLO}_{\text{GO}}$  interaction, the  $0_2^+$  state lies at very high-energy (3.762 MeV).

The  $^{100}\text{Cd}_{52}$  isotope is a good candidate for studying two valence neutron-particle (proton-hole) configurations. For this isotope, the excited  $2_1^+$ ,  $4_2^+$ ,  $6_2^+$ , and  $8_1^+$  states from the G-matrix interaction are comparable with the

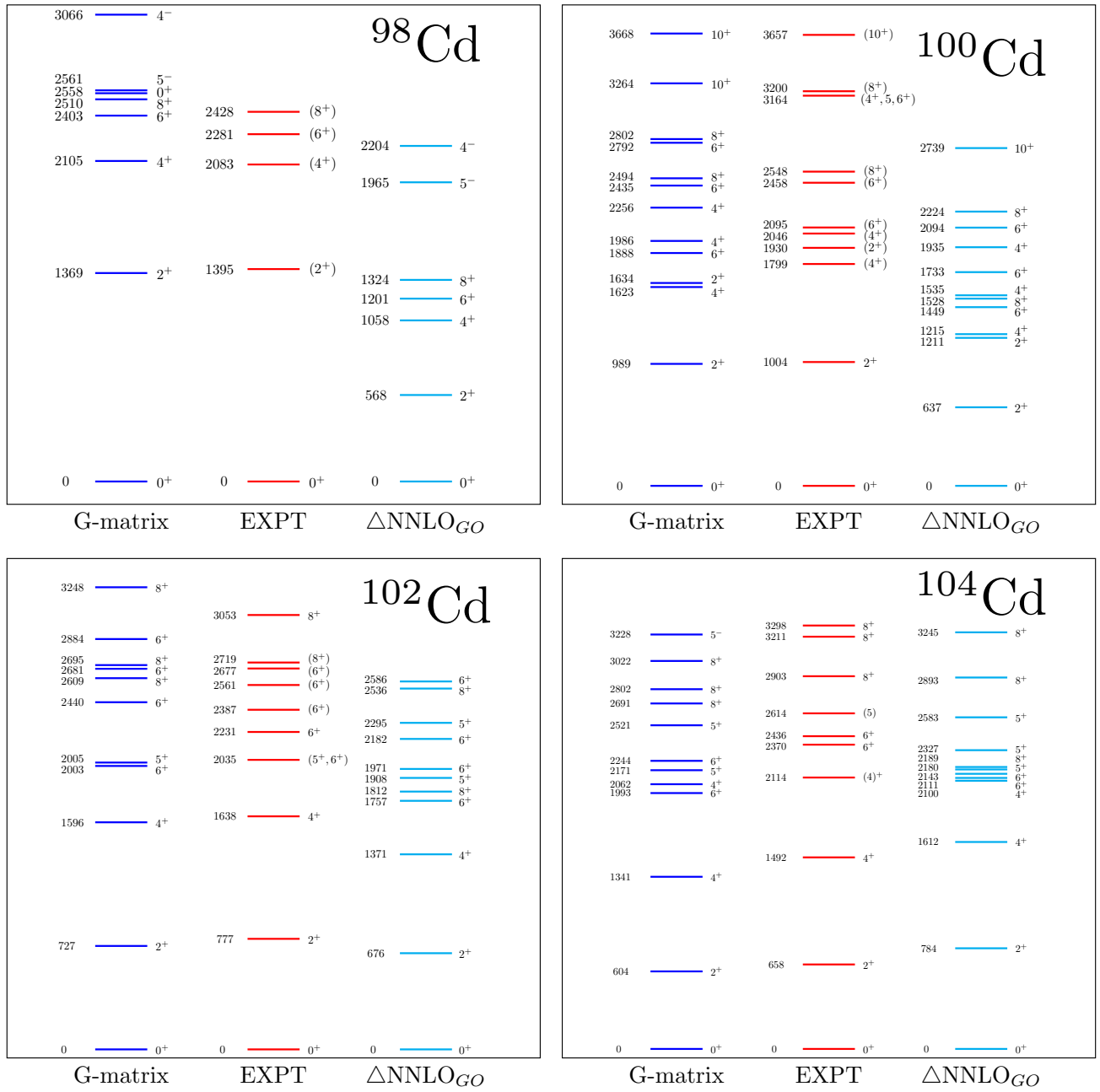


FIG. 2: Comparison between calculated and experimental energy [48] levels for even-even nuclei of  $^{98-104}\text{Cd}$ .

experimental data. The  $4_1^+$  and  $6_1^+$  states lie slightly lower than the tentative experimental data with this interaction. With  $\Delta\text{NNLO}_{\text{GO}}$  interaction these states are compressed. From the G-matrix interaction, the configurations of  $0_1^+$ ,  $2_1^+$  and  $4_1^+$  state are  $\pi(p_{1/2}^2 g_{9/2}^8) \otimes \nu(d_{5/2}^2)_{0+, 2+, 4+}$  with 50%, 55.9% and 67.9% probabilities, respectively. The  $6_1^+$  state is coming with configuration  $\pi(p_{1/2}^2 g_{9/2}^8) \otimes \nu(d_{5/2}^1 g_{7/2}^1)_{6+}$ . From these configurations, it is clear that the yrast  $0_1^+ - 2_1^+ - 4_1^+ - 6_1^+$  states show neutron nature. Which supports the results found in previous works [13, 14]. The excited  $10_1^+$  state lies 0.393 MeV lower than the experimental level from the G-matrix interaction. From the G-matrix interaction, the configuration of the  $10_1^+$  state is  $\pi(p_{1/2}^2 g_{9/2}^8) \otimes \nu(d_{5/2}^1 g_{7/2}^1)$  with 63.1% probability. The little mixing is mainly due to the particle-hole character of the proton-neutron interaction. With  $\Delta\text{NNLO}_{\text{GO}}$  interaction, the  $10_1^+$  state is compressed like other states. The neutron occupancies for  $\Delta\text{NNLO}_{\text{GO}}$  interaction corresponding to  $2_1^+$  state are 1.111, 0.665, 0.076, 0.025, and 0.123 in  $g_{7/2}$ ,  $d_{5/2}$ ,  $d_{3/2}$ ,  $s_{1/2}$  and  $h_{11/2}$  orbitals, respectively. For the G-matrix

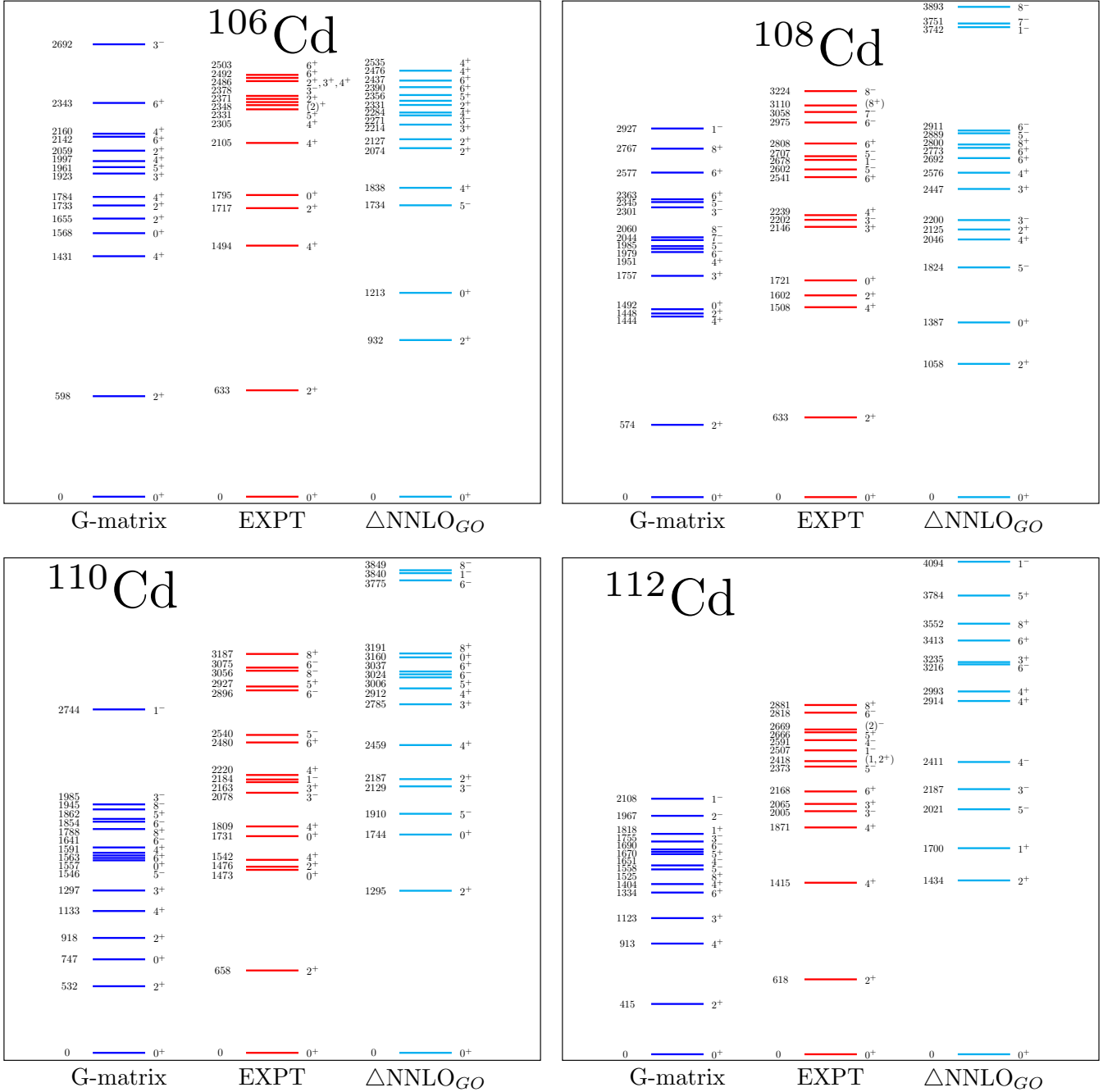


FIG. 3: Comparison between calculated and experimental energy [48] levels for even-even nuclei of  $^{106-112}\text{Cd}$ .

interaction, the neutron occupancies corresponding to  $2_1^+$  state are 1.259, 0.138, 0.446, 0.141, and 0.016 in  $d_{5/2}$ ,  $s_{1/2}$ ,  $g_{7/2}$ ,  $d_{3/2}$  and  $h_{11/2}$  orbitals, respectively. Here, neutron orbital  $d_{5/2}$  is dominating for the G-matrix interaction and  $g_{7/2}$  for  $\Delta\text{NNLO}_{G0}$  interaction. We have also calculated the branching ratios for  $8_1^+ \rightarrow 6_1^+$  and  $8_1^+ \rightarrow 6_2^+$  transitions with the G-matrix interaction ( $e_\pi = 1.7e$ ,  $e_\nu = 1.1e$ ) as 99.96% and 0.04%, respectively. From these results, it seems that the  $6_2^+$  state is fed by weak  $\gamma$ -branches, quite similar to the calculated results in previous work [38]. In Ref. [13], the spacing between calculated  $6_1^+$  and  $8_1^+$  states is reported as 71 keV, our calculated value with G-matrix and  $\Delta\text{NNLO}_{G0}$  interactions are 10 and 130 keV, respectively.

The study of  $^{102}\text{Cd}$  (with  $N = 54$ ) helps for the understanding of  $\pi\nu$  interaction in  $\pi(g_{7/2})$ ,  $\nu(d_{5/2})$ , and  $\nu(g_{7/2})$  orbitals [14]. In  $^{102}\text{Cd}$ , the location of first excited  $2^+$  state is comparable with  $\Delta\text{NNLO}_{G0}$  and the G-matrix interactions. From the G-matrix interaction, the  $4_1^+$  state shows good agreement with the experimental data. But,

this state is compressed by 0.267 MeV than the experimental level with  $\Delta\text{NNLO}_{\text{GO}}$  interaction. The half-life of  $4_1^+$  state should be less than 5.6 ps from the experimental data [48]. Our calculated half-lives are 1.44, 1.69, and 2.29 ps from the G-matrix interaction with effective charges  $(e_\pi, e_\nu) = (1.7, 1.1), (1.4, 1.1)$  and  $(1.4, 0.85)$ , respectively. These calculated half-lives may be useful to compare experimental half-life once it measures accurately for  $4_1^+$  state. In the Cd isotopic chain, the  $^{102}\text{Cd}$  isotope lies in the transitional region between single-particle character (as in nuclei  $^{98}\text{Cd}$ ) and collective vibrational isotopes (with  $N \geq 56$ ). The  $E2$  isomers with spin-parity  $8^+$  are observed in this transitional region. For the isomeric state,  $8_1^+$ , showing good agreement with the G-matrix interaction. With  $\Delta\text{NNLO}_{\text{GO}}$  interaction,  $8_1^+$  state is compressed. The order of  $0_1^+ - 2_1^+ - 4_1^+ - 6_1^+$  states are the same with both interactions. Calculation from the G-matrix interaction favour  $5_1^+$  state for the experimental  $(5^+, 6^+)$  state. With the  $\Delta\text{NNLO}_{\text{GO}}$  interaction,  $6_1^+$  state is compressed but  $5_1^+$  state is comparable with the experimental  $(5^+, 6^+)$  state. In the formation of  $2_1^+$  state, neutron orbital  $d_{5/2}$  dominates with a maximum occupancy of 2.476 for the G-matrix interaction. But, in the case of  $\Delta\text{NNLO}_{\text{GO}}$  interaction neutron orbital  $g_{7/2}$  is dominating.

The  $^{104}\text{Cd}$  shows the typical vibrational behavior and nearly spherical shape at low spins. For this isotope, the excited  $2_1^+$ ,  $4_1^+$  and  $4_2^+$  states reproduced well with  $\Delta\text{NNLO}_{\text{GO}}$  and the G-matrix interactions. From the experimental data, the half-life of  $4_1^+$  state should be less than 4.2 ps [48]. With the three sets of effective charges  $(1.7, 1.1), (1.4, 1.1),$  and  $(1.4, 0.85)$ , the G-matrix calculated half-lives are 2.37, 2.68, and 3.8 ps, respectively. From  $\Delta\text{NNLO}_{\text{GO}}$  interaction, the calculated half-life is 4.16 ps with effective charges  $(1.7, 1.1)$ . We can notice that all calculated half-lives are showing good agreement with the experimental data. The order of  $0_1^+, 2_1^+, 4_1^+, 4_2^+, 6_1^+$  and  $6_2^+$  states are reproduced well with the  $\Delta\text{NNLO}_{\text{GO}}$  interaction. The energy gap between  $4_1^+$  and  $2_1^+$  is comparable with  $\Delta\text{NNLO}_{\text{GO}}$  and the G-matrix interactions as in the experimental data. As reported in Ref. [50], the  $8_1^+$  state decays via  $\gamma$ -transition into  $6_{1,2}^+$  states, this  $8_1^+$  state is slightly compressed with the G-matrix interaction. With  $\Delta\text{NNLO}_{\text{GO}}$  interaction, this state lies lower by 0.714 MeV than the experimental level. In the formation of  $2_1^+$  state, the neutron occupancy is maximum in  $d_{5/2}$  orbital with the G-matrix interaction and  $g_{7/2}$  orbital with  $\Delta\text{NNLO}_{\text{GO}}$  interaction like  $^{100,102}\text{Cd}$ . The excited  $8_3^+$  state is comparable with the experimental level from  $\Delta\text{NNLO}_{\text{GO}}$  interaction. From this interaction, the configuration of  $8_3^+$  state is  $\pi(p_{3/2}^4 p_{1/2}^2 g_{9/2}^8) \otimes \nu(g_{7/2}^2 d_{5/2}^4)$  with 28.7% probability. Here, this state comes from one proton pair breaking in  $g_{9/2}$  orbital. Thus, seniority  $\nu = 2$ . We notice that no low-lying (approximately up to 3.5 MeV) states with negative parity are observed experimentally from  $^{98}\text{Cd}$  to  $^{104}\text{Cd}$ . The reason behind this, there is no significant role of  $h_{11/2}$  orbital in the filling of valence neutrons.

In the cadmium chain,  $^{106}\text{Cd}$  is a good example of the onset of collectivity [51] with a simple structure. This isotope keeps a small but active number of valence nucleons. For this isotope,  $2_1^+$ ,  $4_1^+$ , and  $2_2^+$  states are reproduced well with the G-matrix interaction. Earlier, Benczer-Koller *et al.* [19] performed shell-model calculation for  $^{106}\text{Cd}$  considering  $^{78}\text{Ni}$  as a core. They have calculated the location of  $2_1^+$  and  $4_1^+$  states taking two sets of neutron model spaces. In our work with the G-matrix interaction, the calculated energy levels for  $2_1^+$  and  $4_1^+$  states are close to the experimental data than their results in both cases. With  $\Delta\text{NNLO}_{\text{GO}}$  interaction, these states lie higher than the experimental level. The  $5_1^+$ ,  $6_1^+$  and  $6_2^+$  states are comparable with  $\Delta\text{NNLO}_{\text{GO}}$  interaction. These states are compressed with the G-matrix interaction. The wave function for  $\Delta\text{NNLO}_{\text{GO}}$  interaction, corresponding to  $2_1^+$  state is  $\pi(p_{3/2}^4 p_{1/2}^2 g_{9/2}^8) \otimes \nu(g_{7/2}^4 d_{5/2}^4)$  with maximum probability 21.46%. For the G-matrix interaction, the wave function corresponding to  $2_1^+$  state is  $\pi(p_{1/2}^2 g_{9/2}^8) \otimes \nu(d_{5/2}^4 g_{7/2}^4)$  with maximum probability 26.53%. Here, neutron configuration is same in  $g_{7/2}$  and  $d_{5/2}$  orbitals for  $2_1^+$  state with both interactions. From the G-matrix interaction, the configuration of octupole collective  $3_1^-$  state is  $\pi(p_{1/2}^2 g_{9/2}^8) \otimes \nu(d_{5/2}^3 g_{7/2}^4 h_{11/2}^1)$  with 10.0% probability. It is evident that there are collective structure in  $^{106}\text{Cd}$  with the occupation of atleast single valence neutron in  $h_{11/2}$  orbital.

For  $^{108}\text{Cd}$ , the  $2_1^+$  state is comparable with the G-matrix interaction. With  $\Delta\text{NNLO}_{\text{GO}}$  interaction, these states lie higher than the experimental data. Gade *et al.* [52] established the intruder band in  $^{108}\text{Cd}$  isotope using the Doppler shift attenuation method. The  $0_2^+$  intruder state lies 0.229 and 0.334 MeV lower than the experimental data with the G-matrix and  $\Delta\text{NNLO}_{\text{GO}}$  interactions, respectively. In  $^{108}\text{Cd}$ , the excited  $4_1^+$  and  $2_2^+$  states are two-phonon states. The  $4_1^+$  state is reproduced well, but the  $2_2^+$  state lies 0.154 MeV lower than the experimental level with the G-matrix interaction. With  $\Delta\text{NNLO}_{\text{GO}}$  interaction, the location of  $4_1^+$  and  $2_2^+$  states are overpredicted. Location of the  $3_1^-$  state is showing good agreement with  $\Delta\text{NNLO}_{\text{GO}}$  and the G-matrix interactions. The  $6_1^+$  state is comparable with  $\Delta\text{NNLO}_{\text{GO}}$  interaction. With the G-matrix interaction, this state lies slightly below. It is important to study the lowest quadrupole and octupole modes in  $^{108}\text{Cd}$ . The quadrupole-octupole coupled  $(2^+ \otimes 3^-)$  quintuplet states  $5_1^-$  and  $5_2^-$  are underpredicted with the G-matrix interaction. In case of  $\Delta\text{NNLO}_{\text{GO}}$  interaction, the  $5_1^-$  state is compressed but the location of  $5_2^-$  state is comparable with the experimental data. Another member of this family  $1^-$  state lies 0.249 MeV higher than the experimental level with the G-matrix interaction. This state is coming with configuration  $\pi(p_{1/2}^2 g_{9/2}^8) \otimes \nu(d_{5/2}^4 g_{7/2}^5 h_{11/2}^1)$  and 14.6% probability. The involvement of two neutron orbitals  $h_{11/2}$  and  $g_{7/2}$  with higher single-particle energy push the  $1^-$  state to lie at higher energy. With the G-matrix interaction,  $0_1^+ - 2_1^+ - 4_1^+ - 2_2^+ - 0_2^+ - 3_1^+$  states are in the same order as in the experimental data. In the formation of  $2_1^+$

state,  $d_{5/2}$  orbital is dominating with maximum neutron occupancies of 4.274 for the G-matrix interaction. But, with  $\Delta\text{NNLO}_{\text{GO}}$  interaction  $g_{7/2}$  orbital is dominating with maximum neutron occupancy 4.452.

In the case of  $^{110}\text{Cd}$ , the location of the  $2_1^+$  state is comparable with the experimental data for the G-matrix interaction. With  $\Delta\text{NNLO}_{\text{GO}}$  interaction, this state lies higher than the experimental level. This first excited state decays to the ground state  $0_1^+$  via  $E2$  transition. Our calculated half-life of this state is 12.3 ps from the G-matrix interaction (with effective charges  $e_\pi = 1.7e$ ,  $e_\nu = 1.1e$ ), which is comparable to the experimental half-life 5.42(16) ps [48]. For  $\Delta\text{NNLO}_{\text{GO}}$  interaction, the  $0_2^+$  intruder state lies 0.271 MeV higher than the experimental level with configuration  $\pi(p_{3/2}^4 p_{1/2}^2 g_{9/2}^8) \otimes \nu(g_{7/2}^6 d_{5/2}^6)$  and 10.9% probability. The description of the energy levels of this  $0_2^+$  state is not good with the G-matrix interaction. The  $^{110}\text{Cd}$  isotope is known as collective nuclei showing multiphonon excitations. The order of 2-phonon states  $2_2^+ - 4_1^+ - 0_3^+$  is reproduced with the G-matrix interaction, but these states are compressed. With this interaction, the 2-phonon state  $0_3^+$  lies 0.174 MeV lower than the experimental level. With  $\Delta\text{NNLO}_{\text{GO}}$  interaction, this  $0_3^+$  state ( $\pi(p_{3/2}^4 p_{1/2}^2 g_{9/2}^8) \otimes \nu(g_{7/2}^6 d_{5/2}^4 h_{11/2}^2)$ ) is formed by involvement of two neutrons in higher-lying  $h_{11/2}$  orbital unlike  $0_1^+$  and  $0_2^+$  state. Thus, this state is located at a very high energy than the experimental data. The  $3_1^-$  state is reproduced well with  $\Delta\text{NNLO}_{\text{GO}}$  and the G-matrix interactions. With  $\Delta\text{NNLO}_{\text{GO}}$  interaction, the  $6_1^-$  and  $5_1^-$  states are comparable with the experimental data. But, the order of these states is reversed. These energy levels are compressed with the G-matrix interaction. The  $8_1^+$  state is also well reproduced with  $\Delta\text{NNLO}_{\text{GO}}$  interaction.

For  $^{112}\text{Cd}$ , the order of excited  $0_1^+ - 2_1^+ - 4_1^+$  states are reproduced well with the G-matrix interaction as in the experimental data. The first excited  $2_1^+$  state lies 0.203 MeV lower than the experimental data with this interaction. We have calculated the half-life of this state, which equals 37.17 ps from the G-matrix interaction (with effective charges  $e_\pi = 1.7e$ ,  $e_\nu = 1.1e$ ). Our calculated half-life is slightly higher than the experimental half-life (6.46 ps [48]). Other excited states are compressed with the G-matrix interaction. The octupole state  $3_1^-$  lies 0.182 MeV higher than the experimental data with the  $\Delta\text{NNLO}_{\text{GO}}$  interaction. The energy level of the quadrupole-octupole coupled state  $1^-$  should be near the sum of the energies of the quadrupole and octupole phonon states ( $2_1^+$  and  $3_1^-$ , respectively) [53]. The G-matrix calculated  $1_1^-$  state is underpredicted. But, the sum of the  $2_1^+$  and  $3_1^-$  energies (2.170 MeV) is close to the energy level of the  $1_1^-$  state (2.108 MeV). The  $4_1^-$  state is also a member of quadrupole-octupole coupled quintuplet [28]. The location of the  $4_1^-$  state is 0.180 MeV compressed with the  $\Delta\text{NNLO}_{\text{GO}}$  interaction. From this interaction, the excited  $4_1^-$  state is coming with configuration  $\pi(p_{3/2}^4 p_{1/2}^1 g_{9/2}^9) \otimes \nu(g_{7/2}^6 d_{5/2}^6 h_{11/2}^2)$  and 8.6% probability. Here, the  $4_1^-$  state is formed by the coupling of one unpaired proton in  $p_{1/2}$  orbital and one unpaired proton in  $g_{9/2}$  orbital, having seniority  $\nu = 2$ . It is expected that the negative parity states  $5_1^-$  and  $6_1^-$  are formed by contribution of  $h_{11/2}$  neutron orbital. From the G-matrix interaction, the configuration of  $5_1^-$  and  $6_1^-$  states is  $\pi(p_{1/2}^2 g_{9/2}^8) \otimes \nu(d_{5/2}^4 g_{7/2}^6 d_{3/2}^1 h_{11/2}^3)$  with 10% and 7% probabilities, respectively. In the configuration of both states, we can see that these two negative-parity states ( $5_1^-$  and  $6_1^-$ ) are coming from the coupling of valence neutrons in  $h_{11/2}$  and  $d_{3/2}$  orbitals. For both states, the seniority  $\nu = 2$ .

In the Cd chain, the  $^{114}\text{Cd}$  is situated in the middle of the neutron number  $N = 50$  and  $N = 82$ . In  $^{114}\text{Cd}$ , the excited energy levels are compressed with the G-matrix interaction, but the order of  $0_1^+ - 2_1^+ - 4_1^+ - 3_1^+$  states are reproduced well. The excited  $4_1^-$  state is showing good agreement with the experimental data calculated from the  $\Delta\text{NNLO}_{\text{GO}}$  interaction. With this interaction, the configuration of  $4_1^-$  state is  $\pi(p_{3/2}^4 p_{1/2}^1 g_{9/2}^9) \otimes \nu(g_{7/2}^6 d_{5/2}^6 h_{11/2}^4)$  with 6.4% probability. Here, this  $4_1^-$  state is coming from the coupling of one unpaired proton in  $g_{9/2}$  orbital and one unpaired proton in  $p_{1/2}$  orbital. Thus, the seniority  $\nu = 2$ . The excited  $5_1^-$  state lies 0.219 MeV lower than the experimental data with  $\Delta\text{NNLO}_{\text{GO}}$  interaction. The  $7_1^-$  state is coming with configuration  $\pi(p_{3/2}^4 g_{9/2}^{10}) \otimes (g_{7/2}^8 d_{5/2}^6 d_{3/2}^1 h_{11/2}^1)$  from  $\Delta\text{NNLO}_{\text{GO}}$  interaction. We can see that no valence protons are occupied in  $p_{1/2}$  orbital, and they jump to the  $g_{9/2}$  orbital. This excitation of protons takes more energy to form the  $7^-$  state. So, this state lies at higher energy in comparison to other negative parity states from  $\Delta\text{NNLO}_{\text{GO}}$  interaction. It is expected that the  $h_{11/2}$  neutron orbital plays a dominating role in the mid-shell isotopes of the Cd chain, even at low spin [54]. In the configuration of low-spin states (like  $2_1^+$  state) of  $^{112-114}\text{Cd}$ , we can see that the  $h_{11/2}$  orbital starts to dominate.

For  $^{116}\text{Cd}$ , the order of  $0_1^+ - 2_1^+ - 4_1^+ - 4_2^+$  states are reproduced with the G-matrix interaction. But, these states are compressed. The  $3_1^-$  state is also very compressed with the G-matrix interaction but with  $\Delta\text{NNLO}_{\text{GO}}$  interaction, lies 0.327 MeV higher than the experimental data. The  $5_1^-$  state is comparable with  $\Delta\text{NNLO}_{\text{GO}}$  interaction. From  $\Delta\text{NNLO}_{\text{GO}}$  interaction, the configuration of  $5_1^-$  and  $4_1^-$  states is  $\pi(p_{3/2}^4 p_{1/2}^1 g_{9/2}^9) \otimes \nu(g_{7/2}^8 d_{5/2}^6 h_{11/2}^4)$  with 4.0% and 5.1% probabilities, respectively. From this interaction, both states are formed by the coupling of one unpaired proton in  $p_{1/2}$  orbital and one unpaired proton in  $g_{9/2}$  orbital like  $^{112,114}\text{Cd}$  with seniority  $\nu = 2$ . With the G-matrix interaction, these states are very compressed. We can notice that the energy spectra are compressed with the G-matrix interaction, but the location of  $1_1^+$  state ( $\pi(p_{1/2}^2 g_{9/2}^8) \otimes \nu(d_{5/2}^6 s_{1/2}^1 g_{7/2}^6 d_{3/2}^1 h_{11/2}^4)$ ) is higher in comparison to other states. One can also see that the  $1_1^+$  state ( $\pi(p_{3/2}^3 p_{1/2}^1 g_{9/2}^{10}) \otimes \nu(g_{7/2}^8 d_{5/2}^6 h_{11/2}^4)$ ) is underpredicted with  $\Delta\text{NNLO}_{\text{GO}}$  interaction unlike

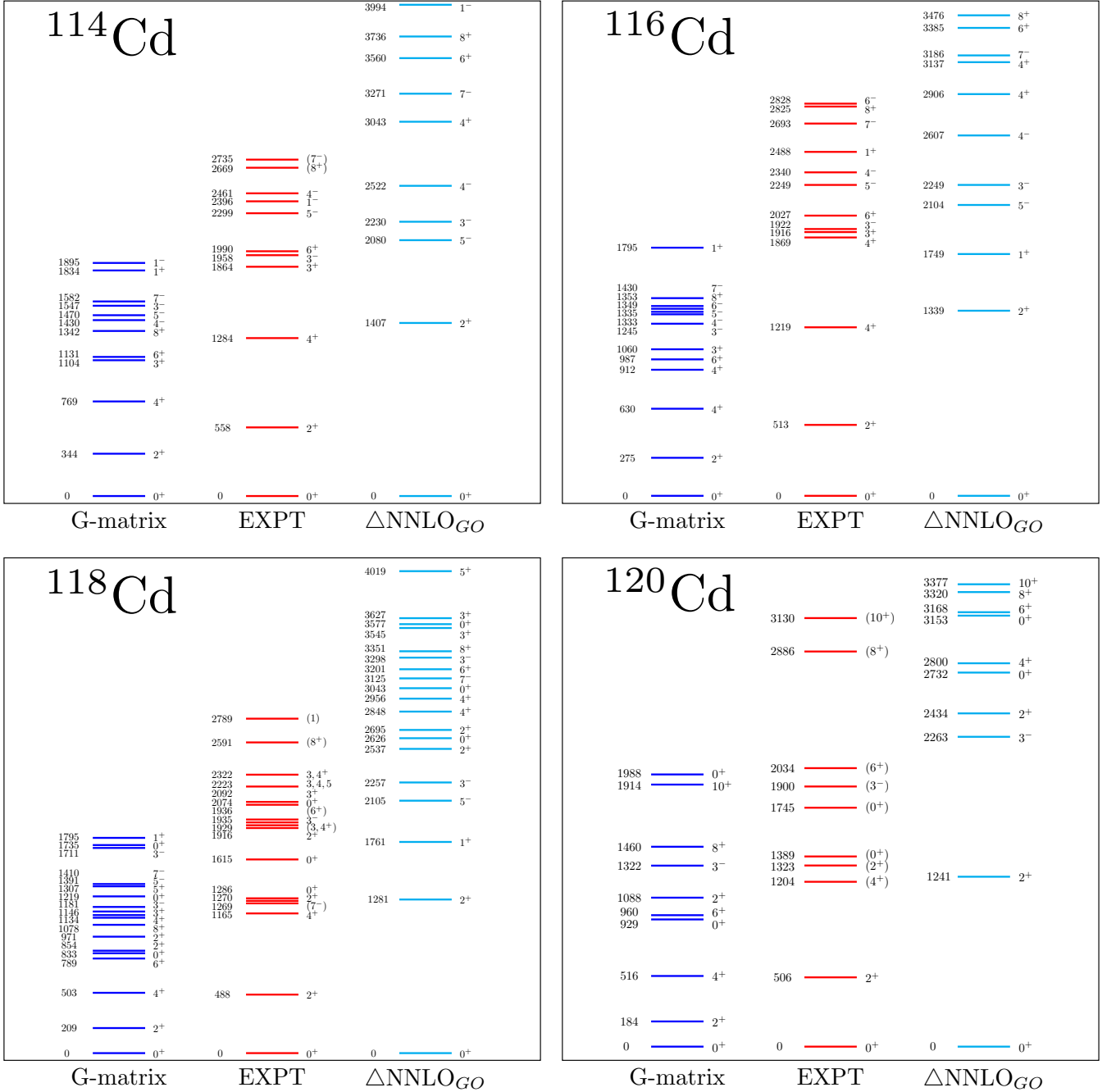


FIG. 4: Comparison between calculated and experimental [48] energy levels for even-even nuclei of  $^{114-120}\text{Cd}$ .

the most of the states are located at higher energy. The reason may be that this  $1_1^+$  state is formed by the coupling of valence protons in low-lying  $p_{3/2}$  and  $p_{1/2}$  orbitals, which compress the location of this state with  $\Delta\text{NNLO}_{G0}$  interaction.

In  $^{118}\text{Cd}$ , the excited  $2_1^+$  state calculated with the G-matrix interaction lies 0.279 MeV lower than the experimental data. The location of 2-phonon states  $4_1^+ - 2_2^+ - 0_2^+$  are also underpredicted with the G-matrix interaction. But, these states are overpredicted with  $\Delta\text{NNLO}_{G0}$  interaction. The excited  $2_{1,2}^+$  states ( $\pi(p_{3/2}^3 p_{1/2}^1 g_{9/2}^{10}) \otimes \nu(g_{7/2}^8 d_{5/2}^6 h_{11/2}^6)$ ) are showing  $\pi(p_{3/2}^{-1} p_{1/2}^{-1})$  character in 34-50 proton model space with  $\Delta\text{NNLO}_{G0}$  interaction. The G-matrix calculated  $7_1^-$  state is comparable with the tentative experimental level at 1.269 MeV. The quadrupole interaction between protons and neutrons is responsible for the excitation energies of intruder states. Earlier, Wang *et al.* [55] studied the intruder

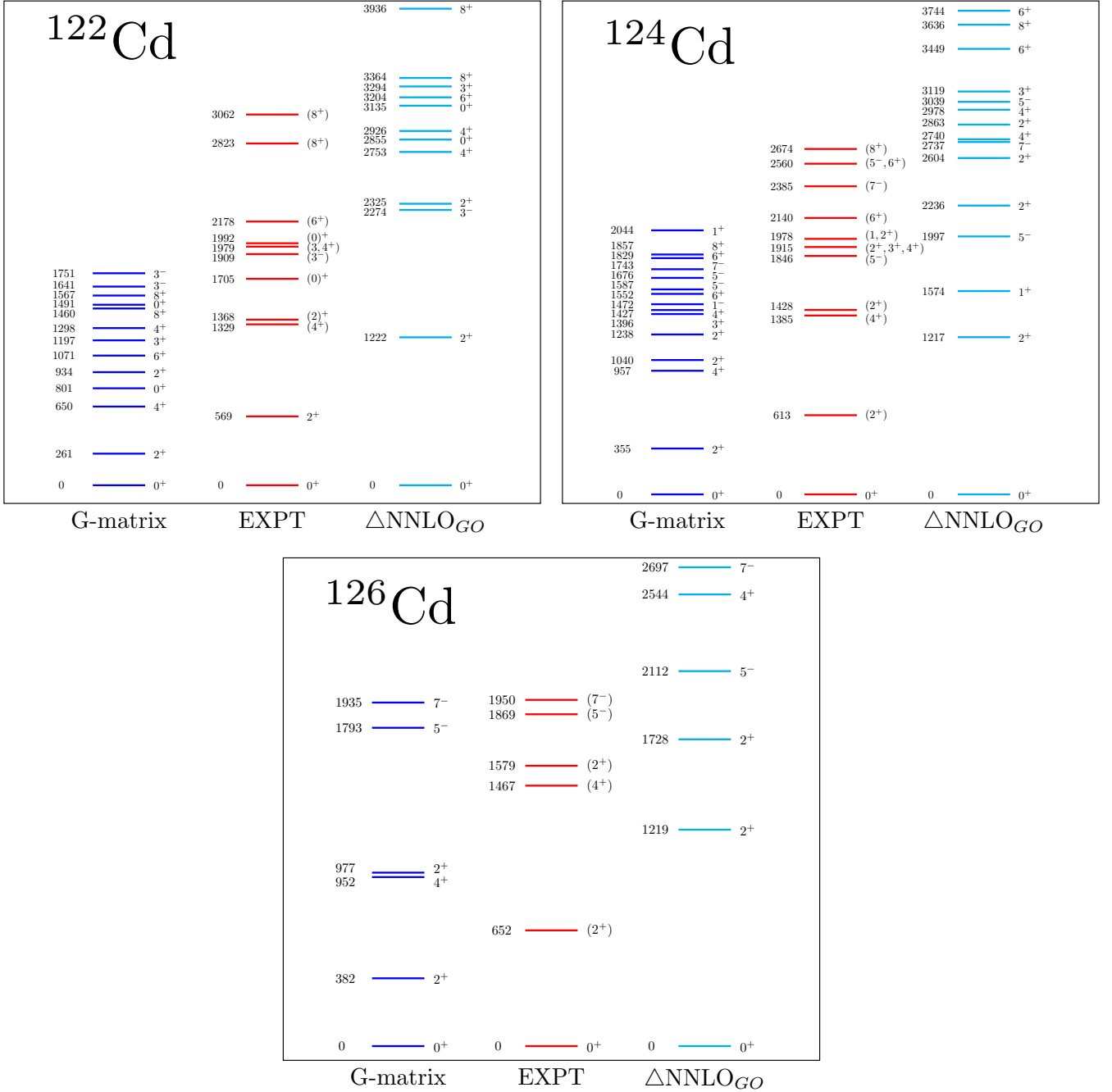


FIG. 5: Comparison between calculated and experimental [48] energy levels for even-even nuclei of  $^{122-126}\text{Cd}$ .

states in  $^{118}\text{Cd}$ . The G-matrix calculated intruder state  $0_3^+$  is compressed by 0.396 MeV than the experimental data. As reported in Ref. [55], the intruder state  $2_3^+$  (at 1916 keV) is compressed with the G-matrix interaction. But, this state lies at very high energy with  $\Delta\text{NNLO}_{GO}$  interaction. In the configuration of the  $2_1^+$  state, the neutron orbitals  $g_{7/2}$  and  $h_{11/2}$  are dominant for  $\Delta\text{NNLO}_{GO}$  interaction. In the neutron-rich region of Cd-isotopes, we can see that the excited energy levels are lying at very high energy with  $\Delta\text{NNLO}_{GO}$  interaction. One reason could be that this chiral interaction is truncated at the two-body level, and the residual three-body term is not included.

For  $^{120}\text{Cd}$ , the order of  $0_1^+ - 2_1^+ - 4_1^+$  states are reproduced well with the G-matrix interaction as in the experimental data. But, the excited  $2_1^+$  and  $4_1^+$  states are compressed with this interaction. The 2-phonon state  $2_2^+$  lies 0.235 MeV lower than the experimental data with the G-matrix interaction. From the G-matrix interaction, the configuration of this state is  $\pi(p_{1/2}^2 g_{9/2}^8) \otimes (d_{5/2}^6 s_{1/2}^2 g_{7/2}^6 d_{3/2}^2 h_{11/2}^6)$  with 28.7% probability, which shows the  $2_2^+$  state comes from

one proton pair breaking in  $g_{9/2}$  orbital with seniority  $\nu = 2$ . This state lies at very high energy with  $\Delta\text{NNLO}_{\text{GO}}$  interaction. The intruder state  $0_3^+$  is overpredicted by 0.243 MeV than the experimental level. With  $\Delta\text{NNLO}_{\text{GO}}$  interaction, excited  $8_1^+$  state lies 0.434 MeV above the experimental level (2.886 MeV). The location of  $10_1^+$  state is 0.247 MeV higher with  $\Delta\text{NNLO}_{\text{GO}}$  interaction from the experimental level. But, this state is underpredicted with the G-matrix interaction. From  $\Delta\text{NNLO}_{\text{GO}}$  and the G-matrix interactions, this state comes with configuration  $\pi(p_{3/2}^4 g_{9/2}^{10}) \otimes (g_{7/2}^8 d_{5/2}^6 d_{3/2}^2 h_{11/2}^6)$  and  $\pi(p_{1/2}^2 g_{9/2}^8) \otimes (d_{5/2}^6 g_{7/2}^6 d_{3/2}^2 h_{11/2}^8)$ , respectively. In the configuration of  $10_1^+$  state there is no proton occupy in  $p_{1/2}$  orbital with  $\Delta\text{NNLO}_{\text{GO}}$  interaction. So, there is an excitation of two valence protons from  $p_{1/2}$  to  $g_{9/2}$  orbital. But, no such type of excitation occurs with the G-matrix interaction, and this  $10_1^+$  state is compressed like other states. The order of  $6_1^+ - 8_1^+ - 10_1^+$  is same with  $\Delta\text{NNLO}_{\text{GO}}$  interaction as in the experimental data.

The low-lying states in  $^{122}\text{Cd}$  have been studied up to  $J^\pi = 8^+$  in Ref. [29]. For this isotope, the excited energy states lie higher than the experimental level with  $\Delta\text{NNLO}_{\text{GO}}$  interaction. The  $3_1^-$  state lies 0.365 MeV higher with  $\Delta\text{NNLO}_{\text{GO}}$  interaction. If we include the three-body forces in this chiral interaction and make some appropriate changes in the adopted model space for our calculations, then we may be able to predict the location of excited states in the neutron-rich isotopes more accurately. With the G-matrix interaction,  $3_1^-$  state is compressed by 0.268 MeV. But, in comparison to other states, the  $3_1^-$  state ( $\pi(p_{1/2}^2 g_{9/2}^8) \otimes (d_{5/2}^6 g_{7/2}^6 d_{3/2}^3 h_{11/2}^9)$ ) lies at high energy with this interaction because it comes from the coupling of higher-lying neutron orbitals  $\nu h_{11/2}$  and  $\nu d_{3/2}$ . On the other side, the  $3_1^-$  state calculated with  $\Delta\text{NNLO}_{\text{GO}}$  interaction is coming with  $\pi(p_{3/2}^3 p_{1/2}^2 g_{9/2}^9) \otimes (g_{7/2}^8 d_{5/2}^6 d_{3/2}^2 h_{11/2}^8)$  configuration. This state is formed by the coupling of valence protons in  $p_{3/2}$  and  $g_{9/2}$  orbitals, which have lower single-particle energies. The  $2_1^+$ ,  $4_1^+$ ,  $6_1^+$  and  $8_1^+$  states are also compressed with the G-matrix interaction. In the formation of  $2_1^+$  state,  $h_{11/2}$  orbital is dominant with maximum neutron occupancies for both interactions.

The level scheme of  $^{124}\text{Cd}$  has been reported in previous works [56, 57]. In  $^{124}\text{Cd}$ , the location of  $2_1^+$ ,  $4_1^+$ ,  $6_1^+$  and  $8_1^+$  states lie higher than the experimental data with  $\Delta\text{NNLO}_{\text{GO}}$  interaction. With  $\Delta\text{NNLO}_{\text{GO}}$  interaction, the  $5_1^-$  state ( $\pi(p_{3/2}^4 p_{1/2}^1 g_{9/2}^9) \otimes (g_{7/2}^8 d_{5/2}^6 d_{3/2}^2 h_{11/2}^{10})$ ) is comparable with the experimental data. This state is formed by the coupling of one valence proton in  $g_{9/2}$  orbital and one valence proton in  $p_{1/2}$  orbital with seniority  $\nu = 2$ . The  $5_1^-$  state is compressed by 0.259 MeV with the G-matrix interaction. But, the  $5_2^-$  state ( $\pi(p_{3/2}^2 p_{1/2}^2 g_{9/2}^{10}) \otimes (g_{7/2}^8 d_{5/2}^6 d_{3/2}^1 h_{11/2}^{11})$ ) is overpredicted with  $\Delta\text{NNLO}_{\text{GO}}$  interaction in comparison to experimentally observed ( $5^-, 6^+$ ) state at 2.560 MeV. This may be due to proton excitation from  $p_{3/2}$  to  $g_{9/2}$  orbital. Another aspect is also important in the formation of the  $5_2^-$  state that this state is showing neutron character and coming from the coupling of higher lying  $\nu h_{11/2}$  and  $\nu d_{3/2}$  orbital, unlike  $5_1^-$  state. The order of excited  $0_1^+ - 2_1^+ - 4_1^+ - 2_2^+$  states are well reproduced by the G-matrix interaction. Like  $^{120,122}\text{Cd}$ , the  $h_{11/2}$  orbital is dominant in the formation of  $2_1^+$  state for both the interactions.

Kautzsch *et al.* [58] calculated the excited energy levels for  $^{126}\text{Cd}$  using shell-model. In our study, the  $2_1^+$  state is compressed by 0.270 MeV with the G-matrix interaction for this isotope. With  $\Delta\text{NNLO}_{\text{GO}}$  interaction, this state lies higher than the experimental data. But, the calculated half-life (6.73 ps) of  $2_1^+$  state with  $\Delta\text{NNLO}_{\text{GO}}$  interaction is close to the experimental half-life 8.9(+27-17) ps. The  $2_2^+$  state is comparable with the  $\Delta\text{NNLO}_{\text{GO}}$  interaction. The  $5_1^-$  state is comparable with the G-matrix interaction. From this interaction, the configuration of  $5_1^-$  state is  $\pi(p_{1/2}^2 g_{9/2}^8) \otimes \nu(d_{5/2}^6 s_{1/2}^1 g_{7/2}^8 d_{3/2}^2 h_{11/2}^{11})$  with 28.6% probability. Here, the  $5_1^-$  state arises from the coupling of unpaired neutrons in  $s_{1/2}$  and  $h_{11/2}$  orbitals. With  $\Delta\text{NNLO}_{\text{GO}}$  interaction, this state lies 0.243 MeV higher than the experimental level. The energy spectra of all states are in the same order with the G-matrix interaction. Hoteling *et al.* [31] suggested a new energy state  $7^-$  at 1950 keV. With the G-matrix interaction, this state is very close to the tentative experimental level with an energy difference of 15 keV. This state comes from  $\pi(p_{1/2}^2 g_{9/2}^8) \otimes \nu(d_{5/2}^6 s_{1/2}^2 g_{7/2}^8 d_{3/2}^3 h_{11/2}^9)$  configuration with 59.3% probability. From  $\Delta\text{NNLO}_{\text{GO}}$  interaction, this state is overpredicted.

For  $^{128}\text{Cd}$ , the prediction of the first excited  $2^+$  state with the G-matrix interaction is comparable. The  $2_1^+$  state lies above than the experimental data with  $\Delta\text{NNLO}_{\text{GO}}$  interaction. From the configurations as shown in Table I, it is clear that the  $2_1^+$  state is formed by the coupling of one valence proton in  $p_{3/2}$  and one valence proton in  $p_{1/2}$  orbitals with  $\Delta\text{NNLO}_{\text{GO}}$  interaction. In the case of the G-matrix interaction, this state comes with one proton pair breaking in  $g_{9/2}$  orbital. But, the seniority is conserved ( $\nu = 2$ ) in all cases. The  $4_1^+$  state lies 0.278 MeV lower than the experimental data with the G-matrix interaction. With  $\Delta\text{NNLO}_{\text{GO}}$  interaction, this state lies at very high energy. The order of  $8_1^+ - 10_1^+$  states is reversed with both interactions. But, the energy gap between  $8_1^+$  and  $10_1^+$  is very close with  $\Delta\text{NNLO}_{\text{GO}}$  and the G-matrix interactions as in the experimental data. As expected, the positive-parity states  $0_1^+ - 8_1^+$  are showing predominant  $\pi(g_{9/2}^-)$  character from the G-matrix interaction. The  $10_1^+$  state shows  $\nu(h_{11/2}^-)$  character with this interaction. The two negative parity states  $5_1^-$  and  $7_1^-$  are coming from  $\pi(p_{1/2}^2 g_{9/2}^8) \otimes \nu(d_{5/2}^6 s_{1/2}^2 g_{7/2}^8 d_{3/2}^3 h_{11/2}^{11})$  configuration with 39.3% and 84.9% probabilities, respectively. Both states are showing  $\nu(d_{3/2}^- h_{11/2}^-)$  character.

In  $^{130}\text{Cd}$ , the order of energy spectra with both interactions is the same as in the experimental data. The ground

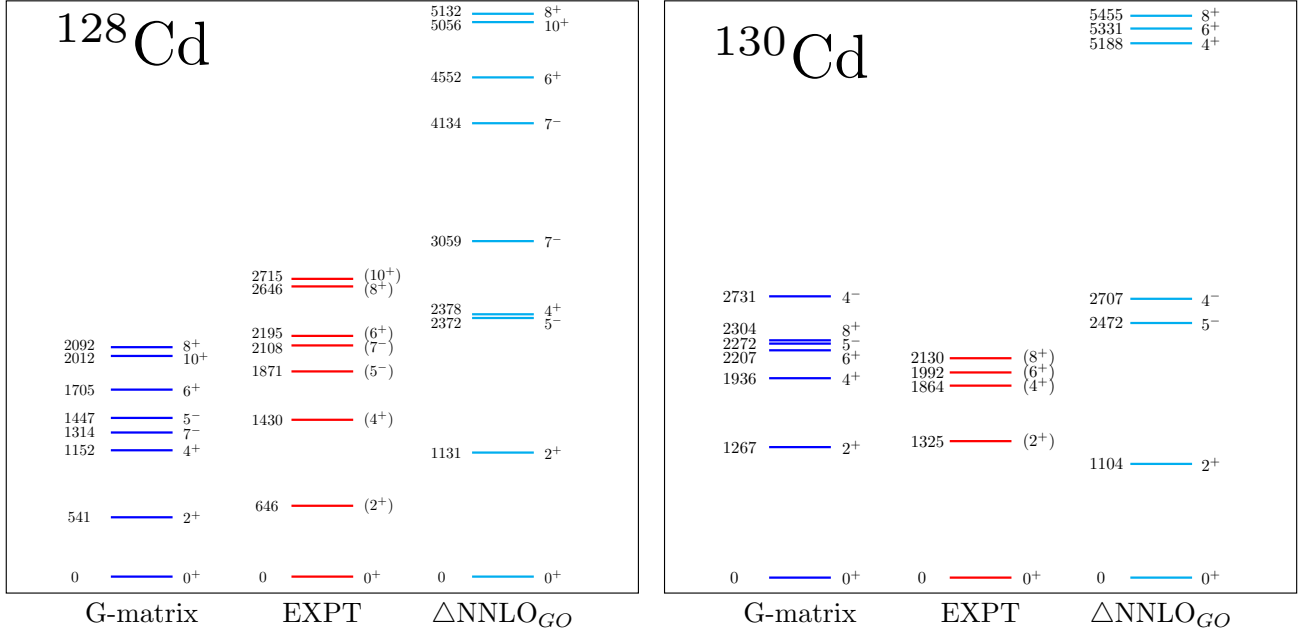


FIG. 6: Comparison between calculated and experimental [48] energy levels for even-even nuclei of  $^{128,130}\text{Cd}$ .

state  $0_1^+$  comes from two different configurations with both interactions. The G-matrix calculated  $0_1^+$  state shows  $\pi(g_{9/2}^{-2})$  nature but showing mixed character with  $\pi(p_{1/2}^{-2})$  configuration from  $\Delta\text{NNLO}_{\text{GO}}$  interaction, also similar result is obtained in Ref. [59]. The location of  $2_1^+$  and  $4_1^+$  states reproduced very well with the G-matrix interaction. With  $\Delta\text{NNLO}_{\text{GO}}$  interaction,  $2_1^+$  state is slightly compressed. The  $6_1^+$  and  $8_1^+$  states lie slightly higher with the G-matrix interaction. With  $\Delta\text{NNLO}_{\text{GO}}$  interaction, these states lie at high energy than the experimental data. The energy gap between  $4_1^+ - 6_1^+$ , and  $6_1^+ - 8_1^+$  states are very close as in the experimental data with  $\Delta\text{NNLO}_{\text{GO}}$  interaction. From both the interactions, these three states ( $4_1^+$ ,  $6_1^+$  and  $8_1^+$ ) are showing  $\pi(g_{9/2}^{-2})$  character. We have also calculated excited  $5_1^-$  and  $4_1^-$  states, which are not observed experimentally yet. For the G-matrix and  $\Delta\text{NNLO}_{\text{GO}}$  interaction, the location of these two states are comparable to each other. Thus, our results may help to compare new experimental data in the future.

We can notice that our energy spectra are deviating from the experimental data from  $^{110}\text{Cd}$  and start to compress up to  $^{120}\text{Cd}$  from the G-matrix interaction. The reason behind this is that when we perform shell-model calculations using realistic interactions and increase the number of particles (neutrons), our results deteriorate rapidly [60]. In the Cd isotopes after the  $^{120}\text{Cd}$ , the increment in neutron particles is treated like a decrease in neutron holes from the magic nuclei  $^{132}\text{Sn}$ . So, our excited states are rising upward with respect to the ground state.

In Fig. 7, we have shown the occupancy of different neutron orbitals corresponding to  $2_1^+$  state from  $N = 50$  to  $N = 82$  in the Cd isotopic chain. The  $d_{5/2}$  and  $g_{7/2}$  orbitals are dominant in the neutron-deficient region for both interactions. With the increase of neutron numbers, occupancy increases in all orbitals. In the mid of the Cd chain, the dominance of the  $h_{11/2}$  orbital can be observed. As we further increase the neutron number, the occupancy of  $h_{11/2}$  orbital becomes more than the other orbitals, which shows the importance of  $h_{11/2}$  orbital in the formation of  $2_1^+$  state in neutron-rich Cd isotopes.

In Fig. 8, we have compared the experimental and theoretical excitation energy ratios of  $4_1^+$  and  $2_1^+$  states in the Cd isotopic chain. We can notice that the  $4_1^+/2_1^+$  energy ratio ( $R_{4/2}$ ) follows the same trend from the  $N = 50$  closed shell toward more collective structures with the G-matrix interaction as in the experimental data. The value of  $R_{4/2}$  ratio is less than 2.0 for  $^{98,100}\text{Cd}$  isotopes with both interactions, which corresponds to a single-particle structure near closed shells. For  $^{102-108}\text{Cd}$  isotopes, the  $R_{4/2}$  ratio lies between 2.0 and 2.6 with the G-matrix interaction, which shows that these isotopes are quasi-deformed. For  $^{106}\text{Cd}$ , the experimental value of  $R_{4/2}$  ratio is 2.360. From our calculation using the G-matrix interaction, the  $R_{4/2}$  ratio is 2.393. The predicted  $R_{4/2}$  ratio from the pure vibrational and rotational model are 2.00 and 3.33, respectively [19]. Here, our calculated result shows good agreement with the experimental data. For  $^{108}\text{Cd}$ , this ratio is 2.516. But, there is a decrement in the  $R_{4/2}$  ratio at  $N = 62$ , which indicates  $^{108}\text{Cd}$  has large deformation. In the neutron-rich isotopes of Cd, the behavior of  $R_{4/2}$  ratio is almost constant with  $\Delta\text{NNLO}_{\text{GO}}$  interaction. But, the G-matrix interaction results are staggering from  $N = 70$  to  $N = 78$ . In  $^{120,124}\text{Cd}$ ,

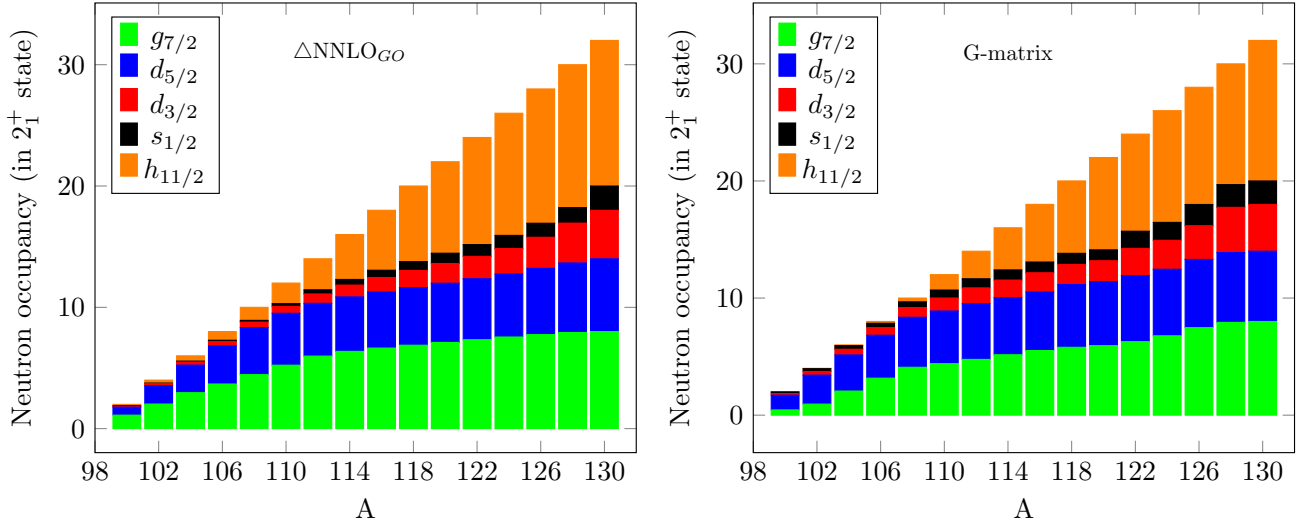


FIG. 7: The occupancy for different neutron orbitals corresponding to excited  $2_1^+$  state in the Cd isotopic chain with  $\Delta\text{NNLO}_{\text{GO}}$ , and the G-matrix interactions.

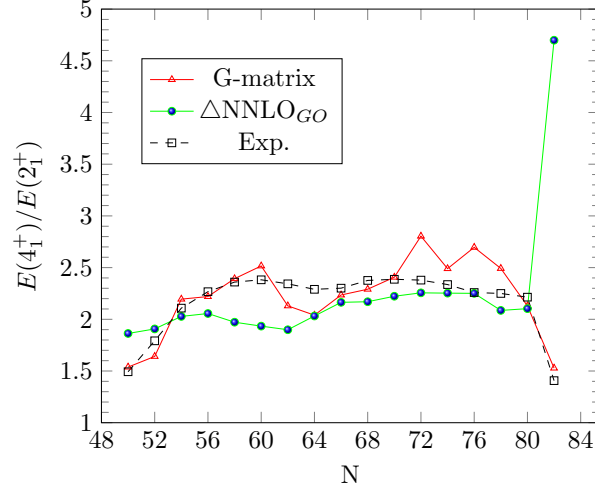


FIG. 8: Comparison of the theoretical and experimental excitation energy ratios of  $4_1^+$  and  $2_1^+$  states in Cd chain. The experimental data are taken from [48].

the configuration of  $4_1^+$  states are  $\pi(p_{1/2}^2 g_{9/2}^8) \otimes \nu(d_{5/2}^6 g_{7/2}^6 d_{3/2}^2 h_{11/2}^8)$  and  $\pi(p_{1/2}^2 g_{9/2}^8) \otimes \nu(d_{5/2}^6 s_{1/2}^2 g_{7/2}^6 d_{3/2}^2 h_{11/2}^{10})$  with the G-matrix interaction, respectively. There are no unpaired nucleons in valence orbitals. So, it needs more energy to form the  $4_1^+$  state, which suddenly increases the  $R_{4/2}$  ratio for  $^{120,124}\text{Cd}$  isotopes. We can also notice that there is a divergence shown at  $N = 82$  with  $\text{NNLO}_{\text{GO}}$  interaction. We need to include more valence neutron orbitals beyond  $N = 82$  to get converged results as in the experimental data.

It is important to add here the chiral effective shell-model interactions provide advances in nuclear structure theory to study medium mass region and help to investigate the unexplored fraction of the nuclear chart. Despite this, these chiral interactions struggle to accurately reproduce the nuclear properties in the neutron-rich region observed from the experiments. We found that the  $\Delta\text{NNLO}_{\text{GO}}$  interaction fails to reproduce the location of energy levels in neutron-rich Cd isotopes. We have tested this chiral interaction for a full isotopic chain for the first time without any truncation. Our study reveals that this interaction needs further improvements and the inclusion of  $3N$  forces for better results.

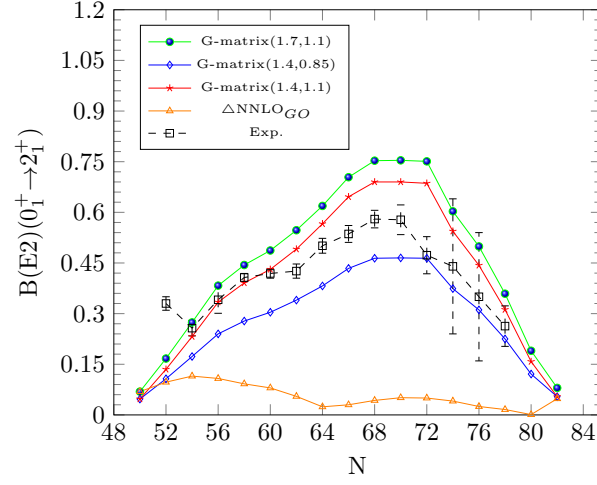


FIG. 9: Behavior of  $B(E2; 0_1^+ \rightarrow 2_1^+)$  values along Cd isotopic chain. The experimental data are taken from [39, 61].

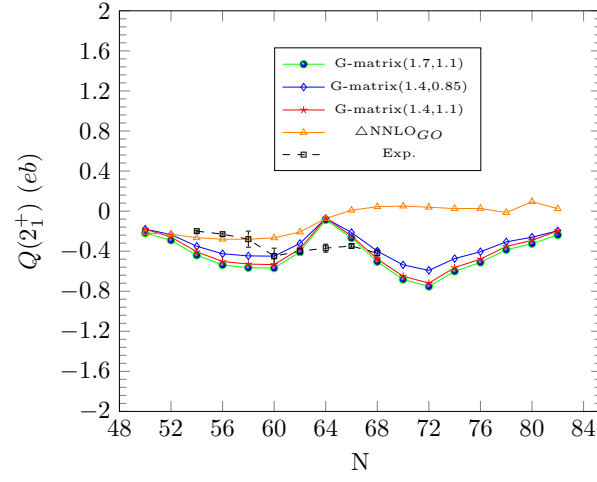


FIG. 10: Electric quadrupole moments for  $2_1^+$  state in Cd isotopic chain. The experimental data for  $^{102,104}\text{Cd}$  and  $^{106-116}\text{Cd}$  are taken from [63] and [64], respectively.

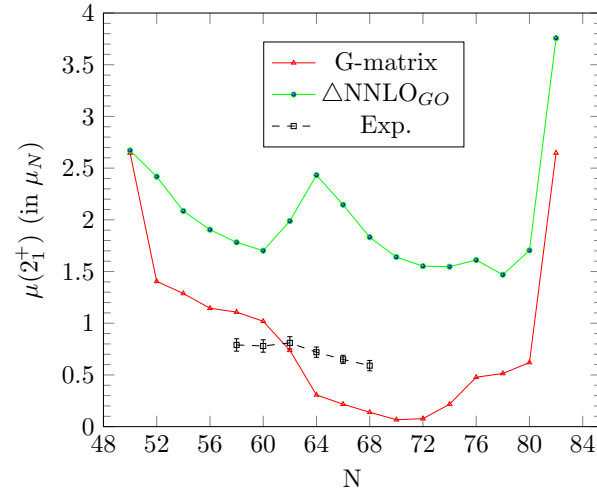


FIG. 11: Magnetic moments for  $2_1^+$  state in Cd isotopic chain. The experimental data are taken from [64].

TABLE II: Comparison of theoretical and experimental  $B(E2)$  transitions in cadmium isotopes. In our calculations we have taken  $(e_p, e_n)=(1.7, 1.1)$  [37]. For the G-matrix interaction, another two sets of effective charges (1.4, 1.1) and (1.4, 0.85) are used [6]. The units are in  $e^2b^2$ .

Isotope	$J_i^\pi \rightarrow J_f^\pi$	$\Delta\text{NNLO}_{\text{GO}}$	G-matrix			Exp.
			(1.7, 1.1)	(1.4, 1.1)	(1.4, 0.85)	
$^{98}\text{Cd}$	$0_1^+ \rightarrow 2_1^+$	0.069	0.069	0.047	0.047	-
	$2_1^+ \rightarrow 4_1^+$	0.032	0.033	0.022	0.022	-
	$4_1^+ \rightarrow 6_1^+$	0.018	0.018	0.012	0.012	0.018(3)
$^{100}\text{Cd}$	$0_1^+ \rightarrow 2_1^+$	0.097	0.167	0.135	0.107	0.33(2)
	$2_1^+ \rightarrow 4_1^+$	0.048	0.047	0.040	0.029	-
	$4_1^+ \rightarrow 6_1^+$	0.029	0.021	0.018	0.013	-
$^{102}\text{Cd}$	$0_1^+ \rightarrow 2_1^+$	0.115	0.274	0.232	0.173	0.257(23)
	$2_1^+ \rightarrow 4_1^+$	0.059	0.143	0.122	0.090	>0.038
	$4_1^+ \rightarrow 6_1^+$	0.035	0.001	0.001	0.001	0.057(45)
$^{104}\text{Cd}$	$0_1^+ \rightarrow 2_1^+$	0.108	0.383	0.334	0.240	0.341(40)
	$2_1^+ \rightarrow 4_1^+$	0.063	0.198	0.175	0.123	0.058 >
	$4_1^+ \rightarrow 6_1^+$	0.035	0.154	0.137	0.096	0.037 >
$^{106}\text{Cd}$	$0_1^+ \rightarrow 2_1^+$	0.092	0.444	0.391	0.278	0.407(12)
	$2_1^+ \rightarrow 4_1^+$	0.068	0.230	0.205	0.143	0.247(32)
	$4_1^+ \rightarrow 6_1^+$	0.017	0.021	0.019	0.013	-
$^{108}\text{Cd}$	$0_1^+ \rightarrow 2_1^+$	0.080	0.487	0.431	0.304	0.419(14)
	$2_1^+ \rightarrow 4_1^+$	0.064	0.255	0.228	0.158	0.225(33)
$^{110}\text{Cd}$	$0_1^+ \rightarrow 2_1^+$	0.055	0.547	0.491	0.340	0.426(21)
	$2_1^+ \rightarrow 4_1^+$	0.048	0.228	0.209	0.141	0.237(51)
$^{112}\text{Cd}$	$0_1^+ \rightarrow 2_1^+$	0.024	0.619	0.566	0.382	0.501(22)
	$2_1^+ \rightarrow 4_1^+$	0.020	0.303	0.278	0.186	0.364(46)
$^{114}\text{Cd}$	$0_1^+ \rightarrow 2_1^+$	0.030	0.704	0.646	0.434	0.536(25)
$^{116}\text{Cd}$	$0_1^+ \rightarrow 2_1^+$	0.043	0.753	0.690	0.464	0.580(26)
$^{118}\text{Cd}$	$0_1^+ \rightarrow 2_1^+$	0.051	0.754	0.690	0.465	0.578(44)
$^{120}\text{Cd}$	$0_1^+ \rightarrow 2_1^+$	0.050	0.751	0.686	0.464	0.473(55)
$^{122}\text{Cd}$	$0_1^+ \rightarrow 2_1^+$	0.041	0.603	0.544	0.374	0.44(20)
$^{124}\text{Cd}$	$0_1^+ \rightarrow 2_1^+$	0.025	0.499	0.443	0.311	0.35(19)
$^{126}\text{Cd}$	$0_1^+ \rightarrow 2_1^+$	0.016	0.359	0.312	0.225	0.263(60)
$^{128}\text{Cd}$	$0_1^+ \rightarrow 2_1^+$	0.010	0.190	0.158	0.121	-
$^{130}\text{Cd}$	$0_1^+ \rightarrow 2_1^+$	0.048	0.080	0.054	0.054	-

TABLE III: Comparison of theoretical and experimental electric quadrupole and magnetic moments in cadmium isotopes. In our calculations we have taken  $(e_p, e_n)=(1.7, 1.1)$ ;  $g_s^p = 3.91$ ,  $g_s^n = -2.678$ . For the G-matrix interaction, another two sets of effective charges (1.4, 1.1) and (1.4, 0.85) are used.

Nuclei	A	$J^\pi$	Q (eb)				Exp.	$\mu$ ( $\mu_N$ )		
			$\Delta\text{NNLO}_{\text{GO}}$	G-matrix				$\Delta\text{NNLO}_{\text{GO}}$	G-matrix	Exp.
				(1.7, 1.1)	(1.4, 1.1)	(1.4, 0.85)				
Cd	98	$2_1^+$	-0.218	-0.219	-0.180	-0.180	-	2.671	2.647	-
		$4_1^+$	-0.119	-0.139	-0.115	-0.115	-	5.293	5.293	-
		$6_1^+$	0.088	0.088	0.072	0.072	-	7.940	7.940	-
		$8_1^+$	0.438	0.438	0.361	0.361	-	10.587	10.587	-
	100	$2_1^+$	-0.231	-0.291	-0.259	-0.234	-	2.418	1.405	-
		$4_1^+$	-0.165	-0.361	-0.330	-0.287	-	4.937	-0.232	-
		$6_1^+$	0.104	-0.572	-0.534	-0.453	-	7.504	0.220	-
		$8_1^+$	0.397	0.659	0.590	0.530	-	10.226	10.154	9.9(5)
	102	$2_1^+$	-0.266	-0.441	-0.406	-0.351	-0.20(1)	2.085	1.288	-
		$4_1^+$	-0.223	-0.527	-0.489	-0.418	-	4.221	2.436	-
		$6_1^+$	0.038	-0.473	-0.437	-0.376	-	6.566	0.572	-
		$8_1^+$	0.575	0.738	0.683	0.586	0.76(9)	9.882	9.117	10.3(2)
	104	$2_1^+$	-0.280	-0.538	-0.503	-0.426	-0.23(1)	1.905	1.145	-
		$4_1^+$	-0.245	-0.675	-0.634	-0.533	-	3.992	1.844	-
	106	$2_1^+$	-0.281	-0.565	-0.529	-0.447	-0.28(8)	1.782	1.108	0.79(6)
		$4_1^+$	-0.255	-0.691	-0.650	-0.545	-	3.740	1.935	0.9(2)
	108	$2_1^+$	-0.267	-0.570	-0.534	-0.450	-0.45(8)	1.702	1.019	0.78(6)
		$4_1^+$	-0.250	-0.604	-0.564	-0.478	-	3.350	1.781	-
	110	$2_1^+$	-0.209	-0.407	-0.378	-0.323	-0.40(4)	1.988	0.738	0.81(6)
		$4_1^+$	-0.202	-0.217	-0.195	-0.181	-	3.648	0.295	-
112	$2_1^+$	-0.074	-0.087	-0.071	-0.072	-0.37(4)	2.432	0.307	0.72(5)	
	$4_1^+$	-0.161	-0.157	-0.132	-0.129	-	3.239	0.179	-	
114	$2_1^+$	0.009	-0.269	-0.248	-0.214	-0.348(12)	2.146	0.217	0.65(4)	
116	$2_1^+$	0.044	-0.505	-0.478	-0.399	-0.42(4)	1.832	0.139	0.59(5)	
118	$2_1^+$	0.050	-0.682	-0.650	-0.537	-	1.640	0.067	-	
120	$2_1^+$	0.039	-0.753	-0.719	-0.592	-	1.552	0.077	-	
122	$2_1^+$	0.025	-0.601	-0.567	-0.474	-	1.547	0.217	-	
124	$2_1^+$	0.027	-0.512	-0.479	-0.406	-	1.611	0.478	-	
126	$2_1^+$	-0.015	-0.386	-0.353	-0.307	-	1.469	0.514	-	
128	$2_1^+$	0.094	-0.325	-0.292	-0.261	-	1.704	0.620	-	
130	$2_1^+$	0.024	-0.238	-0.196	-0.196	-	3.758	2.647	-	

TABLE IV: Comparison between theoretical and experimental  $B(M1)$  (in  $\mu_N^2$ ) values in cadmium isotopes. In our calculations we have taken  $g_s^p = 3.91$ ,  $g_s^n = -2.678$ .

Isotope	$J_i^\pi \rightarrow J_f^\pi$	$\Delta\text{NNLO}_{\text{GO}}$	G-matrix	Exp.
$^{98}\text{Cd}$	$2_2^+ \rightarrow 2_1^+$	0.134	0.818	-
	$4_2^+ \rightarrow 4_1^+$	0.178	0.477	-
$^{100}\text{Cd}$	$2_2^+ \rightarrow 2_1^+$	0.246	0.033	-
	$4_2^+ \rightarrow 4_1^+$	0.267	0.134	-
$^{102}\text{Cd}$	$2_2^+ \rightarrow 2_1^+$	0.162	0.043	-
	$5_1^+ \rightarrow 4_1^+$	0.001	0.002	-
$^{104}\text{Cd}$	$2_2^+ \rightarrow 2_1^+$	0.162	0.043	-
	$4_2^+ \rightarrow 4_1^+$	0.041	0.069	-
$^{106}\text{Cd}$	$2_2^+ \rightarrow 2_1^+$	0.192	0.015	0.013(3)
	$4_2^+ \rightarrow 4_1^+$	0.001	0.001	>0.047
$^{108}\text{Cd}$	$2_2^+ \rightarrow 2_1^+$	0.008	0.025	0.014(9)
	$6_1^- \rightarrow 5_1^-$	0.392	0.021	0.0027(18)
$^{110}\text{Cd}$	$2_2^+ \rightarrow 2_1^+$	0.002	0.095	0.024(4)
	$4_3^+ \rightarrow 4_1^+$	0.040	0.002	0.104(+30-45)
$^{112}\text{Cd}$	$3_1^+ \rightarrow 2_1^+$	0.0001	0.0004	0.003(1)
$^{116}\text{Cd}$	$4_2^+ \rightarrow 4_1^+$	0.432	0.001	0.11(+7-11)
$^{118}\text{Cd}$	$2_2^+ \rightarrow 2_1^+$	0.495	0.010	-
$^{120}\text{Cd}$	$2_2^+ \rightarrow 2_1^+$	0.599	0.0004	-
$^{122}\text{Cd}$	$2_2^+ \rightarrow 2_1^+$	0.605	0.003	-
$^{124}\text{Cd}$	$1_1^+ \rightarrow 0_1^+$	0.059	0.0002	-
$^{126}\text{Cd}$	$2_2^+ \rightarrow 2_1^+$	0.493	0.0001	-

## B. Electromagnetic properties

In this section, we have discussed reduced transition probabilities, quadrupole, and magnetic moments for even Cd isotopes. We have explained the behavior of  $B(E2; 0_1^+ \rightarrow 2_1^+)$  transition for Cd isotopes from  $N = 50$  to  $N = 82$ . The  $B(E2)$  values of the Cd and Sn isotopic chain show similar trends [1]. In the experimental data of  $B(E2)$  values of the Cd chain, there is a dip near  $N = 62$ , as shown in Fig. 9. With our interactions, the neutron orbitals are  $d_{5/2}$ ,  $s_{1/2}$ ,  $d_{3/2}$ ,  $g_{7/2}$  and  $h_{11/2}$  in the order of increasing single-particle energies, respectively. The asymmetry near  $N = 62$  is because  $d_{5/2}$ ,  $s_{1/2}$  and  $d_{3/2}$  orbitals lie lower than remaining  $g_{7/2}$  and  $h_{11/2}$  orbitals. Before  $N = 62$ ,  $d_{5/2}$  orbital is dominating and after that  $h_{11/2}$  orbital is dominating. Our results from the G-matrix interaction are in good agreement with the experimental trend. We have used three sets of effective charges ( $e_\pi, e_\nu$ ) for calculating  $B(E2; 0_1^+ \rightarrow 2_1^+)$  values with the G-matrix interaction. The effective charges (1.7, 1.1) are taken from Ref. [37]. Another two sets (1.4, 1.1) and (1.4, 0.85) are taken from Ref. [6]. We can notice that our results with the effective charges (1.4, 1.1) are comparable with the experimental trend before the mid-shell. With the effective charges (1.4, 0.85), our results show good agreement with the experiment in the neutron-rich region of Cd-isotopes. With  $\Delta\text{NNLO}_{\text{GO}}$  interaction, the shape of the inverted parabola is very compressed.

We have also calculated  $B(E2)$  transitions for other states, reported in Table II. In  $^{98}\text{Cd}$ ,  $B(E2; 4_1^+ \rightarrow 6_1^+)$  value is reproduced well and equals to  $0.018 e^2 b^2$  with  $\Delta\text{NNLO}_{\text{GO}}$  and the G-matrix ( $e_p = 1.7$ ,  $e_n = 1.1$ ) interactions. Park *et al.* [62] studied the  $6_1^+$  isomeric state in a decay spectroscopy experiment with half-life,  $T_{1/2} = 13(2)$  ns. With the G-matrix ( $e_p = 1.7$ ,  $e_n = 1.1$ ) interaction, the calculated half-life of the  $6_1^+$  state is 1.92 ns. In the case of even

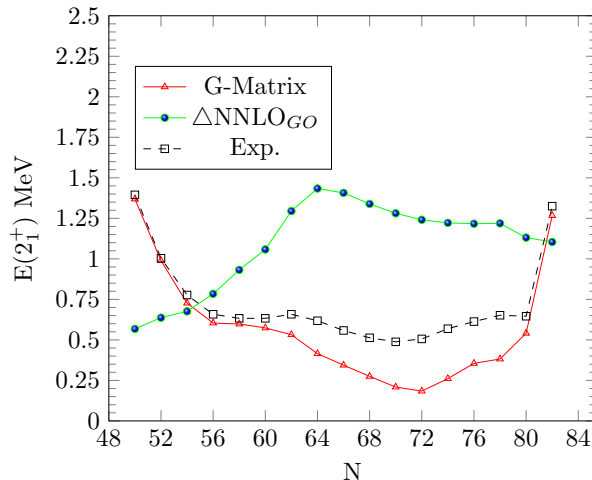


FIG. 12: Comparison of the experimental excitation energy of the  $2_1^+$  states for Cd isotopic chain with our results.

$^{106-112}\text{Cd}$  isotopes, the  $B(E2; 2_1^+ \rightarrow 4_1^+)$  values calculated from the G-matrix ( $e_p = 1.7$ ,  $e_n = 1.1$ ) interaction are showing good agreement with the experimental data [48].

In most cases,  $B(E2)$  values apart from  $B(E2; 0_1^+ \rightarrow 2_1^+)$  are in good agreement with the G-matrix interaction. But, with  $\Delta$ NNLO<sub>GO</sub> interaction, we need to include the effects of  $NNN$  forces to reproduce better results.

The trend of the  $11/2^-$  quadrupole moments for odd  $^{111-129}\text{Cd}$  isotopes have been studied in previous works [65, 66]. In  $^{106-116}\text{Cd}$  isotopes, the experimental data are available for  $Q(2_1^+)$  values. We have used shell-model interpreted data of  $Q(2_1^+)$  [63] for  $^{102,104}\text{Cd}$ . We have compared our results with the experimental data for even Cd isotopic chain as shown in Fig. 10. One can notice that the  $Q(2_1^+)$  values show nearly constant behavior for  $^{102-106}\text{Cd}$  isotopes. Results from  $\Delta$ NNLO<sub>GO</sub> interaction are comparable for these isotopes. Experimentally, there is a dip of  $Q(2_1^+)$  value at  $^{108}\text{Cd}$ . After that, the trend of  $Q(2_1^+)$  is almost constant up to  $^{116}\text{Cd}$ . For  $^{98,100}\text{Cd}$  isotopes,  $Q(2_1^+)$  values are very close to each other with all interactions. But, they have not been observed in the experiment yet. Experimental data are not available for the electric quadrupole moment of  $2_1^+$  state in neutron-rich even Cd isotopes. In the future, our results may be helpful in comparing upcoming experimental results in Cd isotopes.

For  $^{102}\text{Cd}$ , the experimental  $Q(8_1^+)$  value is close to our result with the G-matrix interaction ( $e_p = 1.7$ ,  $e_n = 1.1$ ). We have also calculated electric quadrupole moments for other states, as reported in Table III.

For magnetic moments of  $2_1^+$  state, the experimental data are available only for  $^{106-116}\text{Cd}$  isotopes like quadrupole moments. The trend of our calculated results for  $\mu(2_1^+)$  values is not similar to the experimental data as shown in Fig. 11. But, some  $\mu(2_1^+)$  values are close to the experimental data calculated with the G-matrix interaction. In the case of  $^{100,102}\text{Cd}$  isotopes, the experimental  $\mu(8_1^+)$  show good agreement with our results. For  $^{106}\text{Cd}$ , the  $\mu(4_1^+)$  value is two times higher than the experimental value with the G-matrix interaction. With  $\Delta$ NNLO<sub>GO</sub> interaction, this value is overpredicted. In Table III, we have also reported magnetic moments for other states where the experimental data are not available.

For the even Cd isotopic chain, the experimental data of  $B(M1)$  values are available only for a few states. We have reported  $B(M1)$  transitions for these isotopes in Table IV. In case of  $^{106}\text{Cd}$ ,  $B(M1; 2_2^+ \rightarrow 2_1^+)$  value is reproduced well with the G-matrix interaction. For  $\Delta$ NNLO<sub>GO</sub> interaction, our calculated  $B(M1)$  values are higher than the experimental data.

### C. Variation in the excitation energy of $2_1^+$ states from $N = 50$ to $N = 82$

In this section, we have explained the nature of excitation energy of the  $2_1^+$  state for the Cd isotopic chain. We can notice that there is a small change at  $N = 62$  in the variation of the experimental excitation energy of  $2_1^+$  state, as shown in Fig. 12. The cause may be a sub-shell gap in the single-particle energies of neutron orbitals. When neutrons start occupying in the valence space, first  $d_{5/2}$ ,  $s_{1/2}$  and  $d_{3/2}$  orbitals prefer to filling. As we further increase the neutrons around  $N = 62$ , the dominance of  $h_{11/2}$  orbital will be started. So, the change in variation of  $2_1^+$  state energy is related to the change in the filling of neutron orbitals. At  $N = 82$ , there is the neutron shell closure. Hence, the energy of the excited  $2_1^+$  state suddenly increases at  $N = 82$ .

TABLE V: Comparison between theoretical and experimental  $B(E3; 0_1^+ \rightarrow 3_1^-)$  (in  $e^2b^3$ ) values in cadmium isotopes. In our calculations we have taken  $(e_p, e_n)=(1.7, 1.1)$ . For the G-matrix interaction, another two sets of effective charges (1.4, 1.1) and (1.4, 0.85) are also used.

Isotope	$J_i^\pi \rightarrow J_f^\pi$	$\Delta\text{NNLO}_{\text{GO}}$	G-matrix			Exp.
			(1.7, 1.1)	(1.4, 1.1)	(1.4, 0.85)	
$^{106}\text{Cd}$	$0_1^+ \rightarrow 3_1^-$	0.021	0.001	0.001	$0.007 \times 10^{-1}$	0.16(4)
$^{108}\text{Cd}$	$0_1^+ \rightarrow 3_1^-$	0.030	$0.003 \times 10^{-1}$	$0.003 \times 10^{-1}$	$0.002 \times 10^{-1}$	0.142(21)
$^{110}\text{Cd}$	$0_1^+ \rightarrow 3_1^-$	0.041	0.002	0.002	0.001	0.120(23)
$^{112}\text{Cd}$	$0_1^+ \rightarrow 3_1^-$	0.055	$0.096 \times 10^{-4}$	$0.096 \times 10^{-4}$	$0.057 \times 10^{-4}$	0.120(25)
$^{114}\text{Cd}$	$0_1^+ \rightarrow 3_1^-$	0.060	$0.675 \times 10^{-3}$	$0.675 \times 10^{-3}$	$0.403 \times 10^{-3}$	0.166(27)
$^{116}\text{Cd}$	$0_1^+ \rightarrow 3_1^-$	0.060	0.001	$0.902 \times 10^{-3}$	$0.538 \times 10^{-3}$	0.100(11)
$^{118}\text{Cd}$	$0_1^+ \rightarrow 3_1^-$	0.058	0.003	0.003	0.002	-
$^{120}\text{Cd}$	$0_1^+ \rightarrow 3_1^-$	0.055	$0.004 \times 10^{-1}$	$0.004 \times 10^{-1}$	$0.002 \times 10^{-1}$	-
$^{122}\text{Cd}$	$0_1^+ \rightarrow 3_1^-$	0.050	$0.677 \times 10^{-4}$	$0.007 \times 10^{-2}$	$0.004 \times 10^{-2}$	-

The trend for excited  $2_1^+$  energy states for  $N = 50 - 82$  reproduced well with the G-matrix interaction. With  $\Delta\text{NNLO}_{\text{GO}}$  interaction, these energy states lie higher than the experimental data. We need some modifications to reproduce a better trend in the variation of  $2_1^+$  state energies.

#### D. Octupole collective $3^-$ states in even-even Cd isotopes

The study of  $3^-$  states are important for the understanding of the octupole vibrational mode of a nucleus. Low-lying  $3^-$  octupole states are found in  $^{106-122}\text{Cd}$  isotopes. They decay via electromagnetic transitions to  $0^+$  and  $2^+$  states. In Fig. 13, we have compared the experimental trend of the  $3^-$  state in the Cd chain with our results. We can see that the results with  $\Delta\text{NNLO}_{\text{GO}}$  interaction are very close to the experimental data. The  $3_1^-$  states calculated with the G-matrix interaction deviate in the mid-shell.

In  $^{106}\text{Cd}$ , the octupole  $3_1^-$  state is experimentally observed at the energy of 2.378 MeV. The location of this state is comparable with  $\Delta\text{NNLO}_{\text{GO}}$  interaction. For  $\Delta\text{NNLO}_{\text{GO}}$  interaction, the wave function corresponding to  $3_1^-$  state is  $\pi(p_{3/2}^3 p_{1/2}^2 g_{9/2}^9) \otimes \nu(g_{7/2}^4 d_{5/2}^4)$  with 16.9% probability. With the G-matrix interaction, this state lies higher than the experimental data. Here, the  $3_1^-$  state is formed by the coupling of one unpaired proton in  $p_{3/2}$  orbital and one unpaired proton in  $g_{9/2}$  orbital with  $\Delta\text{NNLO}_{\text{GO}}$  interaction. Thus, the seniority  $\nu = 2$ .

The G-matrix and  $\Delta\text{NNLO}_{\text{GO}}$  interactions are able to reproduce octupole  $3_1^-$  state in  $^{108}\text{Cd}$ . The wave functions corresponding to  $3_1^-$  state are  $\pi(p_{3/2}^3 p_{1/2}^2 g_{9/2}^9) \otimes \nu(g_{7/2}^6 d_{5/2}^4)$  and  $\pi(p_{1/2}^2 g_{9/2}^8) \otimes \nu(d_{5/2}^4 g_{7/2}^5 h_{11/2}^1)$  with probabilities 12.4% and 15.8% for  $\Delta\text{NNLO}_{\text{GO}}$  and the G-matrix interactions, respectively. In the case of  $\Delta\text{NNLO}_{\text{GO}}$  interaction,  $3_1^-$  state is arising from the coupling of single unpaired protons in  $g_{9/2}$  and  $p_{3/2}$  orbitals. For the G-matrix interaction, this state is formed by the coupling of one unpaired neutron in  $h_{11/2}$  orbital with one unpaired neutron in  $g_{7/2}$  orbital. In both cases, the seniority is conserved and equal to 2.

For  $^{110}\text{Cd}$ , the octupole  $3_1^-$  state is showing good agreement with the experimental data for  $\Delta\text{NNLO}_{\text{GO}}$  and the G-matrix interactions. For  $\Delta\text{NNLO}_{\text{GO}}$  interaction, configuration of  $3_1^-$  state is  $\pi(p_{3/2}^3 p_{1/2}^2 g_{9/2}^9) \otimes \nu(g_{7/2}^6 d_{5/2}^6)$  with 11.8% probability. The neutron occupancies in  $g_{7/2}$ ,  $d_{5/2}$ ,  $d_{3/2}$ ,  $s_{1/2}$  and  $h_{11/2}$  orbitals are 5.250, 4.276, 0.514, 0.191 and 1.769, respectively. This  $3_1^-$  state is formed by the coupling of single unpaired protons in  $g_{9/2}$  and  $p_{3/2}$  orbitals. Thus, the seniority  $\nu = 2$ .

In case of  $^{112,114,116}\text{Cd}$  isotopes, the configurations of  $3_1^-$  state from  $\Delta\text{NNLO}_{\text{GO}}$  interaction are  $\pi(p_{3/2}^3 p_{1/2}^2 g_{9/2}^9) \otimes \nu(g_{7/2}^6 d_{5/2}^6 h_{11/2}^2)$ ,  $\pi(p_{3/2}^3 p_{1/2}^2 g_{9/2}^9) \otimes \nu(g_{7/2}^6 d_{5/2}^6 h_{11/2}^4)$  and  $\pi(p_{3/2}^3 p_{1/2}^2 g_{9/2}^9) \otimes \nu(g_{7/2}^8 d_{5/2}^6 h_{11/2}^4)$  with 8.5%, 6.1% and 4.7% probabilities, respectively. For these three isotopes, this octupole  $3^-$  state arises from the coupling of one unpaired proton in  $p_{3/2}$  orbital and one unpaired proton in  $g_{9/2}$  orbital. Thus, the seniority is 2.

For  $^{118}\text{Cd}$ ,  $3_1^-$  state is very compressed with G-matrix interaction. With  $\Delta\text{NNLO}_{\text{GO}}$  interaction, this state is 0.322

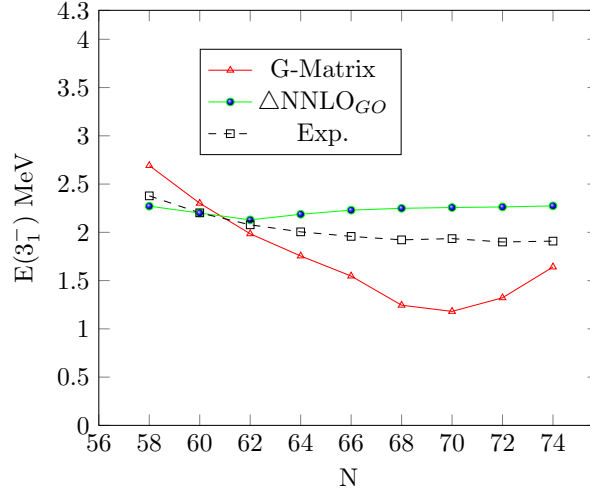


FIG. 13: Comparison of the experimental excitation energy of the octupole collective  $3_1^-$  states for  $^{106-122}\text{Cd}$  isotopes with our results.

MeV higher than the experimental level with configuration  $\pi(p_{3/2}^3 p_{1/2}^2 g_{9/2}^9) \otimes \nu(g_{7/2}^8 d_{5/2}^6 h_{11/2}^6)$  and 4.7% probability. The neutron occupancies are 6.813, 4.672, 1.328, 0.701, 6.485 in  $g_{7/2}$ ,  $d_{5/2}$ ,  $d_{3/2}$ ,  $s_{1/2}$  and  $h_{11/2}$  orbitals, respectively. Here,  $h_{11/2}$  orbital starts to dominate in the formation of the  $3_1^-$  state.

In case of  $^{120}\text{Cd}$ , location of  $3_1^-$  state is 0.363 MeV higher than the experimental data with  $\Delta$ NNLO<sub>GO</sub> interaction. For this interaction, the wave function corresponding to  $3_1^-$  state is  $\pi(p_{3/2}^3 p_{1/2}^2 g_{9/2}^9) \otimes \nu(g_{7/2}^8 d_{5/2}^6 h_{11/2}^8)$  with maximum probability 4.4%.

For  $^{122}\text{Cd}$ , the wave functions corresponding to octupole  $3_1^-$  state are  $\pi(p_{3/2}^3 p_{1/2}^2 g_{9/2}^9) \otimes \nu(g_{7/2}^8 d_{5/2}^6 d_{3/2}^2 h_{11/2}^8)$  and  $\pi(p_{1/2}^2 g_{9/2}^8) \otimes \nu(d_{5/2}^6 g_{7/2}^6 d_{3/2}^3 h_{11/2}^9)$  with probabilities 5.3% and 27.3% for  $\Delta$ NNLO<sub>GO</sub> and the G-matrix interactions, respectively. Here,  $\nu h_{11/2}$  orbital is dominant for both interactions with maximum occupancies of 8.998 ( $\Delta$ NNLO<sub>GO</sub>) and 8.912 (G-matrix interaction), respectively.

For the octupole  $3_1^-$  state, we can notice that the seniority remains constant ( $\nu = 2$ ) with  $\Delta$ NNLO<sub>GO</sub> interaction in the Cd chain. From this interaction, the  $3_1^-$  states are showing  $\pi(p_{3/2}^{-1} g_{9/2}^{-1})$  character for  $^{106-122}\text{Cd}$  isotopes. We have also calculated  $B(E3; 0_1^+ \rightarrow 3_1^-)$  transitions in  $^{106-122}\text{Cd}$  isotopes and compared them with the experimental data [67] as reported in Table V. With  $\Delta$ NNLO<sub>GO</sub> interaction, our calculated  $B(E3; 0_1^+ \rightarrow 3_1^-)$  values are slightly lower than the experimental data. The G-matrix calculated results are very small.

### E. $8^+$ isomeric states in Cd chain

Many theoretical and experimental investigations have been performed to study isomeric states in the different mass regions of the nuclear chart [12, 68–73]. The  $8^+$  isomers have been observed experimentally in  $^{98-104,130}\text{Cd}$  isotopes. In this section, we briefly discussed the  $B(E2)$  transitions, neutron occupancies, configurations of the  $8^+$  isomeric states, and their g-factor values in the Cd chain.

In  $^{98}\text{Cd}$ , the wave function corresponding to  $8_1^+$  isomeric state is  $\pi(p_{1/2}^2 g_{9/2}^8)$  for the G-matrix interaction with 100% probability. Here, the  $8_1^+$  state is formed by one proton pair breaking of the  $g_{9/2}$  orbital. So, the seniority  $\nu = 2$ . Our result for  $B(E2; 8_1^+ \rightarrow 6_1^+)$  transition is comparable to the experimental data. The experimental and the G-matrix calculated (with  $e_p = 1.4$ ,  $e_n = 1.1$ )  $B(E2; 8_1^+ \rightarrow 6_1^+)$  values are 0.0038(4)  $e^2 b^2$  and 0.0034  $e^2 b^2$ , respectively. As reported in Table VI, the small value of  $B(E2; 8_1^+ \rightarrow 6_1^+)$  support  $8_1^+$  state is an isomeric state with half-life 0.39  $\mu\text{s}$ , calculated from  $\Delta$ NNLO<sub>GO</sub> interaction and corresponding experimental half-life is 0.154(16)  $\mu\text{s}$  [48].

The experimentally observed  $8_1^+$  isomeric state in  $^{100}\text{Cd}$  (with a total half-life 62(6) ns [48]) is reproduced well with the G-matrix interaction. For the G-matrix interaction, the wave function corresponding to this state is  $\pi(p_{1/2}^2 g_{9/2}^8) \otimes \nu(d_{5/2}^2)$  with 55.0% probability and the neutron occupancies for  $8_1^+$  state are 1.185, 0.079, 0.573, 0.143 and 0.020 in  $d_{5/2}$ ,  $s_{1/2}$ ,  $g_{7/2}$ ,  $d_{3/2}$  and  $h_{11/2}$  orbitals, respectively. With the G-matrix interaction,  $8_1^+$  state arises because of one pair breaking in  $g_{9/2}$  proton orbital, thus  $\nu = 2$ . From the G-matrix interaction, the configuration of  $6_1^+$  state is

TABLE VI: Comparison of theoretical and experimental  $B(E2)$  transitions (in  $e^2b^2$ ) of  $8_1^+$  isomeric states in Cd isotopes. The calculated half-lives are also reported. In our calculations we have taken  $e_p = 1.7e$  and  $e_n = 1.1e$ . For the G-matrix interaction, another set of effective charge (1.4, 1.1) is also used [6].

Isotope	$J_i^\pi \rightarrow J_f^\pi$	$B(E2)$				$T_{1/2}$			
		$\Delta\text{NNLO}_{\text{GO}}$	G-matrix		Exp.	$\Delta\text{NNLO}_{\text{GO}}$	G-matrix		Exp.
			(1.7, 1.1)	(1.4, 1.1)			(1.7, 1.1)	(1.4, 1.1)	
$^{98}\text{Cd}$	$8_1^+ \rightarrow 6_1^+$	0.005	0.005	0.0034	0.0038(4)	0.39 $\mu\text{s}$	0.81 $\mu\text{s}$	1.19 $\mu\text{s}$	0.154(16) $\mu\text{s}$
$^{100}\text{Cd}$	$8_1^+ \rightarrow 6_1^+$	0.008	0.0002	0.0001	0.000042(5)	2.19 $\mu\text{s}$	$4.33 \times 10^{-3} \mu\text{s}$	$5.78 \times 10^{-3} \mu\text{s}$	0.073 $\mu\text{s}$
	$8_1^+ \rightarrow 6_2^+$	$0.0196 \times 10^{-4}$	0.0079	0.0061	0.0061(+33-28)	79.85 $\mu\text{s}$	10.03 $\mu\text{s}$	13.101 $\mu\text{s}$	0.413 $\mu\text{s}$
$^{102}\text{Cd}$	$8_1^+ \rightarrow 6_1^+$	0.009	0.007	0.006	0.000017(3)	12.2 $\mu\text{s}$	$97.5 \times 10^{-6} \mu\text{s}$	$1.17 \times 10^{-4} \mu\text{s}$	0.093 $\mu\text{s}$
	$8_1^+ \rightarrow 6_2^+$	$0.838 \times 10^{-4}$	0.004	0.0029	-	6.65 $\mu\text{s}$	0.12 $\mu\text{s}$	0.15 $\mu\text{s}$	-
	$8_1^+ \rightarrow 6_3^+$	$0.192 \times 10^{-4}$	0.0006	0.0005	-	0.426 $\mu\text{s}$	49.3 $\mu\text{s}$	55.25 $\mu\text{s}$	0.067 $\mu\text{s}$
$^{104}\text{Cd}$	$8_1^+ \rightarrow 6_1^+$	0.0083	0.1087	0.096	0.0015(5)	2.37 $\mu\text{s}$	$3.12 \times 10^{-6} \mu\text{s}$	$3.55 \times 10^{-6} \mu\text{s}$	$8.6 \times 10^{-4} \mu\text{s}$
	$8_1^+ \rightarrow 6_2^+$	0.0004	0.0001	$0.005 \times 10^{-2}$	0.0002(1)	621.45 $\mu\text{s}$	$37.07 \times 10^{-3} \mu\text{s}$	$63.5 \times 10^{-3} \mu\text{s}$	$11.43 \times 10^{-3} \mu\text{s}$
$^{130}\text{Cd}$	$8_1^+ \rightarrow 6_1^+$	0.006	0.006	0.004	-	0.33 $\mu\text{s}$	1.12 $\mu\text{s}$	1.65 $\mu\text{s}$	0.220(30) $\mu\text{s}$

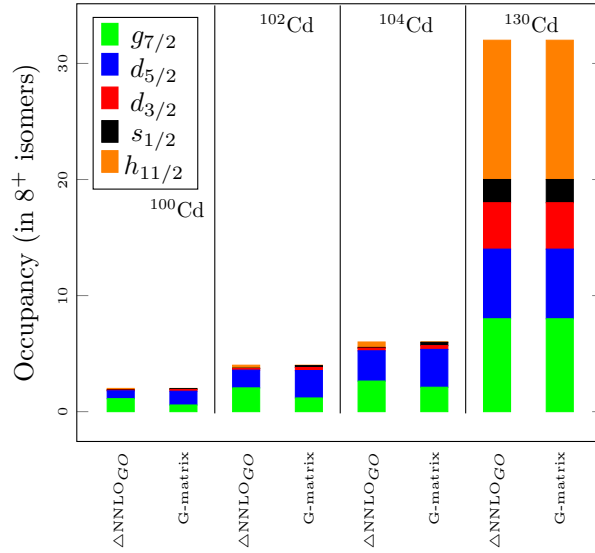


FIG. 14: Neutron occupancies in  $8^+$  isomeric states for  $^{100,102,130}\text{Cd}$  isotopes.

$\pi(p_{1/2}^2 g_{9/2}^8)_{0+} \otimes \nu(g_{7/2}^1 d_{5/2}^1)_{6+}$  with 82.4% probability, which shows predominant neutron character of the  $6_1^+$  state. But, the configuration of  $6_2^+$  state is  $\pi(p_{1/2}^2 g_{9/2}^8)_{6+} \otimes \nu(d_{5/2}^2)_{0+}$  with 73.3% probability. Here, the  $6_2^+$  state is formed by one proton pair breaking in  $g_{9/2}$  orbital. So, the  $6_2^+$  state has more resemblance to the  $8_1^+$  isomer in  $^{100}\text{Cd}$ . For this isotope, there are a difference in  $B(E2; 8_1^+ \rightarrow 6_1^+)$  values of our calculated result (with the G-matrix interaction) and the experimental data. But, the  $B(E2; 8_1^+ \rightarrow 6_2^+)$  transition is comparable with the experimental value from this interaction. Clark *et al.* [38] reported the experimental branching ratios of  $B(E2)$  transitions in  $8_1^+$  state in  $^{100}\text{Cd}$ . We have used their data to find the partial half-lives of  $8_1^+$  state as reported in Table VI.

For  $^{102}\text{Cd}$ , the configuration of  $8_1^+$  isomeric state is  $\pi(p_{1/2}^2 g_{9/2}^8) \otimes \nu(g_{7/2}^2 d_{5/2}^2)$  from the G-matrix interaction with 31.7% probability. With this interaction,  $8_1^+$  state is formed by one pair breaking in  $g_{9/2}$  proton orbital like  $^{98,100}\text{Cd}$  isotopes, thus the seniority  $\nu = 2$ . For the G-matrix interaction, the neutron occupancies are 1.178, 2.361, 0.264, 0.159, and 0.039, corresponding to  $g_{7/2}$ ,  $d_{5/2}$ ,  $d_{3/2}$ ,  $s_{1/2}$  and  $h_{11/2}$  orbitals, respectively. For the experimental partial

TABLE VII: The calculated g-factor (in  $\mu_N$ ) for the experimentally observed  $8^+$  isomeric states in Cd isotopes compared to the experimental data. The shell-model calculations are performed with  $g_l^\pi = 1.0$ ,  $g_l^\nu = 0.0$ ;  $g_s^\pi = 3.91$ ,  $g_s^\nu = -2.678$ ;  $e_\pi = 1.7e$ ,  $e_\nu = 1.1e$ .

Isotope	$J^\pi$	$\Delta\text{NNLO}_{\text{GO}}$	G-matrix	Exp.
$^{98}\text{Cd}$	$8^+$	1.323	1.323	-
$^{100}\text{Cd}$	$8^+$	1.278	1.269	1.24(6)
$^{102}\text{Cd}$	$8^+$	1.235	1.140	1.29(3)
$^{104}\text{Cd}$	$8^+$	1.240	0.392	-
$^{130}\text{Cd}$	$8^+$	1.323	1.323	-

half-lives of  $8_1^+$  state, we have used the experimental branching ratios of  $B(E2)$  transitions in  $8_1^+$  state from the Ref. [15].

In  $^{104}\text{Cd}$ , the  $8_1^+$  isomeric state is observed with half-life of 0.8(+2-1) ns [74]. For the G-matrix interaction, the configuration of this state is  $\pi(p_{1/2}^2 g_{9/2}^8) \otimes \nu(d_{5/2}^4 g_{7/2}^2)$  with 39.6% probability. This isomeric state comes from one proton pair breaking in  $g_{9/2}$  orbital. Hence, seniority  $\nu = 2$ . We have used the experimental data of branching ratios from the Ref. [75] to calculate the partial half-lives of  $8_1^+$  state.

In  $^{130}\text{Cd}$ , the  $8_1^+$  isomeric state lies slightly higher with an energy difference of 0.174 MeV with the G-matrix interaction. For this interaction, the configuration of  $8_1^+$  state is  $\pi(p_{1/2}^2 g_{9/2}^8) \otimes \nu(d_{5/2}^6 s_{1/2}^2 g_{7/2}^8 d_{3/2}^4 h_{11/2}^{12})$  with 100% probability. Here, this  $8_1^+$  isomeric state is also arising because of one pair breaking of  $g_{9/2}$  proton orbital and  $\nu = 2$ . With  $\Delta\text{NNLO}_{\text{GO}}$  interaction, the half-lives of  $8_1^+$  isomeric state is 0.33  $\mu\text{s}$ . This value is close to the experimental half-life (0.220(30)  $\mu\text{s}$  [48]) of  $8_1^+$  state.

In the vicinity of the doubly magic nuclei  $^{132}\text{Sn}$ , microsecond isomers are studied in previous work [76]. Scherillo *et al.* [30] investigated microsecond isomers in the neutron-rich region of the Cd isotopes using the LOHENGRIN mass spectrometer. But, the expected  $8^+$  isomeric states were not observed. Our shell-model calculations predict the half-lives of the  $8_1^+$  states in the ns range for  $^{126,128}\text{Cd}$ . The half-lives with our calculations are much shorter, which may explain the non-observation of microsecond isomers in  $^{126,128}\text{Cd}$  isotopes.

In Fig. 14, we have shown the occupancy of neutron orbitals corresponding to  $8_1^+$  isomeric states in  $^{100-104,130}\text{Cd}$  isotopes with  $\Delta\text{NNLO}_{\text{GO}}$  and the G-matrix interactions. For  $^{100-104}\text{Cd}$  isotopes,  $d_{5/2}$  and  $g_{7/2}$  neutron orbitals are dominant corresponding to  $8_1^+$  isomeric states. In the case of  $^{130}\text{Cd}$ , there is a shell closure at  $N = 82$ .

The g-factor for  $8_1^+$  isomeric states in Cd isotopes are reported in Table VII. The experimental data of the g-factors for  $8_1^+$  isomeric states in Cd isotopes are available only for  $^{100-102}\text{Cd}$ . With our calculations, the g-factor is almost constant for  $8_1^+$  isomeric states in  $^{98-104,130}\text{Cd}$  isotopes (except in the case of  $^{104}\text{Cd}$  with the G-matrix interaction), which supports the additivity rule for nuclear magnetic moments. The measurement of the g-factor explains the purity of a configuration, and the contribution of the component corresponding to a particular state [69]. We expect that the main configuration of an isomeric state will be pure. The  $8_1^+$  isomeric states in  $^{98-104,130}\text{Cd}$  isotopes are formed by the pair breaking in the same proton orbital. We have calculated magnetic moment corresponding to  $g_{9/2}$  orbital ( $\mu(g_{9/2})$ ) using formula  $\mu = [g_l + g_s/2]\mu_N$ . After that, we calculated the g-factor value  $g = \mu(g_{9/2})/j$ , which equals 1.510. This value is close to our calculated g-factor values with both interactions. Thus, our calculations support these  $8_1^+$  isomers show  $(\pi g_{9/2})^2$  character.

## V. SUMMARY AND CONCLUSIONS

In the present work, we have investigated the low-lying states in  $^{98-130}\text{Cd}$  isotopes. Systematic shell-model calculations have been performed for Cd isotopic chain from  $N = 50$  to  $N = 82$  with  $\Delta\text{NNLO}_{\text{GO}}$  and the G-matrix interactions. From our calculations for  $^{98-104}\text{Cd}$  isotopes with the G-matrix interactions, we can see that the energy gap between  $0_1^+$  and  $2_1^+$  state increases as we move from  $^{104}\text{Cd}$  to  $^{98}\text{Cd}$ . This indicates we are approaching the collective vibrational to the closed shell region. The behavior of  $4_1^+/2_1^+$  energy ratio ( $R_{4/2}$ ) has been studied in the Cd chain. We have shown the trend of  $B(E2; 0_1^+ \rightarrow 2_1^+)$  transition along Cd isotopic chain and tried to explain the asymmetry near  $N = 62$ . We have also calculated the other electromagnetic properties like electric quadrupole moments,  $B(M1)$  transitions, and magnetic moments for even  $^{98-130}\text{Cd}$  isotopes. We have studied different aspects

of the octupole collective  $3_1^-$  states in Cd isotopes and compared the  $B(E3; 0_1^+ \rightarrow 3_1^-)$  transition values with the corresponding experimental data. The properties of experimentally observed  $8^+$  isomeric states in  $^{98-104,130}\text{Cd}$  isotopes have been investigated using shell-model calculations. Thus, our study also supports the occurrence of E2 isomerism in  $8_1^+$  states in neutron-deficient Cd isotopes. We have also reported the g-factor values for the  $8_1^+$  isomeric states in Cd isotopes and tried to explain the purity of the configuration of these states.

## VI. ACKNOWLEDGEMENTS

We acknowledge financial support from MHRD, the Government of India, and SERB (India), CRG/2019/000556. We would like to thank the National Supercomputing Mission (NSM) for providing computing resources of ‘PARAM Ganga’ at the Indian Institute of Technology Roorkee, implemented by C-DAC and supported by the Ministry of Electronics and Information Technology (MeitY) and Department of Science and Technology (DST), Government of India. We would also like to thank Professor Larry Zamick for useful discussions during this work.

- 
- [1] M. Siciliano *et al.*, Lifetime measurements in the even-even  $^{102-108}\text{Cd}$  isotopes, *Phys. Rev. C* **104**, 034320 (2021).
  - [2] C. Vaman, C. Andreoiu, D. Bazin, A. Becerril, B. A. Brown *et al.*,  $Z = 50$  Shell Gap near  $^{100}\text{Sn}$  from Intermediate-Energy Coulomb Excitations in Even-Mass  $^{106-112}\text{Sn}$  Isotopes, *Phys. Rev. Lett.* **99**, 162501 (2007).
  - [3] T. Togashi, Y. Tsunoda, T. Otsuka, N. Shimizu, and M. Honma, Novel Shape Evolution in Sn Isotopes from Magic Numbers 50 to 82, *Phys. Rev. Lett.* **121**, 062501 (2018).
  - [4] B. S. Nara Singh, Z. Liu, R. Wadsworth, H. Grawe *et al.*,  $16^+$  Spin-Gap Isomer in  $^{96}\text{Cd}$ , *Phys. Rev. Lett.* **107**, 172502 (2011).
  - [5] T. Faestermann, M. Górska, H. Grawe, The structure of  $^{100}\text{Sn}$  and neighbouring nuclei, *Prog. Part. Nucl. Phys.* **69**, 85 (2013).
  - [6] A. P. Zuker, Quadrupole dominance in the light Sn and in the Cd isotopes, *Phys. Rev. C* **103**, 024322 (2021).
  - [7] A. Banu *et al.*,  $^{108}\text{Sn}$  studied with intermediate-energy Coulomb excitation, *Phys. Rev. C* **72**, 061305(R) (2005).
  - [8] P. Doornenbal *et al.*, Enhanced strength of the  $2_1^+ \rightarrow 0_{g.s.}^+$  transition in  $^{114}\text{Sn}$  studied via Coulomb excitation in inverse kinematics, *Phys. Rev. C* **78**, 031303(R) (2008).
  - [9] I. O. Morales, P. Van Isacker and I. Talmi, Generalized seniority and  $E2$  transitions in the tin isotopes, *Phys. Lett. B* **703**, 606 (2011).
  - [10] B. Maheshwari and A. K. Jain, Odd tensor electric transitions in high-spin Sn-isomers and generalized seniority, *Phys. Lett. B* **753**, 122 (2016).
  - [11] R. Kumar *et al.*, Enhanced  $0_{g.s.}^+ \rightarrow 2_1^+$   $E2$  transition strength in  $^{112}\text{Sn}$ , *Phys. Rev. C* **81**, 024306 (2010).
  - [12] P.C. Srivastava, B. Bhoy and M.J. Ermamatov, Different seniority states of  $^{119-126}\text{Sn}$  isotopes: shell-model description, *Prog. of Theor. and Exp. Phys.* **2019**, 103D01 (2019).
  - [13] M. Górska *et al.*, The decay of the  $I^\pi = 8^+$  isomer in  $^{100}\text{Cd}$ -neutron particle and proton hole states, *Z. Phys. A* **350**, 181 (1994).
  - [14] D. Alber *et al.*, Nuclear structure study of the neutron deficient cadmium isotopes  $^{100,101,102}\text{Cd}$ , *Z. Phys. A* **344**, 1 (1992).
  - [15] K. P. Lieb, D. Kast, A. Jungclaus, I. P. Johnstone, G. de Angelis, C. Fahlander, M. de Poli, P. G. Bizzeti, A. Dewald, R. Peusquens, H. Tiesler, M. Gorska, and H. Grawe, Proton versus neutron excitations in the high-spin spectrum of  $^{102}\text{Cd}$ , *Phys. Rev. C* **63**, 054304 (2001).
  - [16] N. Boelaert, A. Dewald, C. Fransen, J. Jolie, A. Linnemann, B. Melon, O. Moller, N. Smirnova, and K. Heyde, Low-spin electromagnetic transition probabilities in  $^{102,104}\text{Cd}$ , *Phys. Rev. C* **75**, 054311 (2007); N. Smirnova (private communication).
  - [17] G. A. Müller *et al.*, High-spin structure and electromagnetic transition strengths in  $^{104}\text{Cd}$ , *Phys. Rev. C* **64**, 014305 (2001).
  - [18] A. J. Simons *et al.*, Investigation of antimagnetic rotation in light Cadmium nuclei:  $^{106,108}\text{Cd}$ , *Phys. Rev. C* **72**, 024318 (2005).
  - [19] N. Benczer-Koller *et al.*, Magnetic moment and lifetime measurements of Coulomb-excited states in  $^{106}\text{Cd}$ , *Phys. Rev. C* **94**, 034303 (2016).
  - [20] P. Fan *et al.*, g-factor measurements of high spin states in  $^{108}\text{Cd}$ , *Hyperfine Interact.* **230**, 155 (2015).
  - [21] J. Kumpulainen, R. Julin, J. Kantele, A. Passoja, W. H. Trzaska, E. Verho, J. Vaaramaki, D. Cutoiu, and M. Ivascu, Systematic study of low-spin states in even Cd nuclei, *Phys. Rev. C* **45**, 640 (1992).
  - [22] A. Gade, and P. von Brentano, Evidence for the complete quadrupole-octupole coupled multiplet in  $^{108}\text{Cd}$ , *Phys. Rev. C* **66**, 014304 (2002).
  - [23] K. Nomura, and J. Jolie, Structure of even-even cadmium isotopes from the beyond-mean-field interacting boson model, *Phys. Rev. C* **98**, 024303 (2018).
  - [24] F. Corminboeuf, T. B. Brown, L. Genilloud, C. D. Hannant, J. Jolie, J. Kern, N. Warr, and S. W. Yates, Structures and lifetimes of states in  $^{110}\text{Cd}$ , *Phys. Rev. C* **63**, 014305 (2000).
  - [25] M. Piiparinen *et al.*, Lifetimes of yrast states in  $^{110}\text{Cd}$ , *Nucl. Phys. A* **565**, 671 (1993).

- [26] P. H. Regan, A. E. Stuchbery, and S. S. Anderssen, Measurement of the g-factor of the yrast  $10^+$  state in  $^{110}\text{Cd}$ , *Nucl. Phys. A* **591**, 533 (1995).
- [27] P. E. Garrett, K. L. Green, H. Lehmann, J. Jolie, C. A. McGrath, M. Yeh, and S. W. Yates, Properties of  $^{112}\text{Cd}$  from the  $(n, n'\gamma)$  reaction: Lifetimes and transition rates, *Phys. Rev. C* **75**, 054310 (2007).
- [28] D. S. Jamieson *et al.*, Quadrupole-octupole coupled states in  $^{112}\text{Cd}$  populated in the  $^{111}\text{Cd}(d, p)$  reaction, *Phys. Rev. C* **90**, 054312 (2014).
- [29] N. V. Zamfir, R. L. Gill, D. S. Brenner, R. F. Casten, and A. Wolf, Study of low-spin states in  $^{122}\text{Cd}$ , *Phys. Rev. C* **51**, 98 (1995).
- [30] A. Scherillo, J. Genevey, J. A. Pinston, A. Covello, H. Faust, A. Gargano, R. Orlandi, G. Simpson, I. Tsekhanovich, and N. Warr, Neutron-rich In and Cd isotopes close to the doubly magic  $^{132}\text{Sn}$ , *Phys. Rev. C* **70**, 054318 (2004).
- [31] N. Hotelling *et al.*, Onset of isomers in  $^{125,126,127,128}\text{Cd}$  and weakened neutron-neutron interaction strength, *Phys. Rev. C* **76**, 044324 (2007).
- [32] D. Lascar, R. Klawitter, C. Babcock, E. Leistenschneider, S. R. Stroberg, B. R. Barquest, A. Finlay, M. Foster, A. T. Gallant, P. Hunt, J. Kelly, B. Kootte, Y. Lan, S. F. Paul, M. L. Phan, M. P. Reiter, B. Schultz, D. Short, J. Simonis, C. Andreoiu, M. Brodeur, I. Dillmann, G. Gwinner, J. D. Holt, A. A. Kwiatkowski, K. G. Leach, and J. Dilling, Precision mass measurements of  $^{125-127}\text{Cd}$  isotopes and isomers approaching the  $N = 82$  closed shell, *Phys. Rev. C* **96**, 044323 (2017).
- [33] R. Dunlop *et al.*, Half-lives of neutron-rich  $^{128-130}\text{Cd}$ , *Phys. Rev. C* **93**, 062801(R) (2016).
- [34] I. Dillmann, K.-L. Kratz, A. Wöhr, O. Arndt, B. A. Brown, P. Hoff, M. Hjorth-Jensen *et al.*,  $N = 82$  Shell Quenching of the Classical  $r$ -Process “Waiting-Point” Nucleus  $^{130}\text{Cd}$ , *Phys. Rev. Lett.* **91**, 162503 (2003).
- [35] T. Schmidt, K. L. G. Heyde, A. Blazhev, and J. Jolie, Shell-model-based deformation analysis of light cadmium isotopes, *Phys. Rev. C* **96**, 014302 (2017).
- [36] A. Blazhev, M. Górska, H. Grawe, J. Nyberg, M. Palacz, E. Caurier, O. Dorvaux, A. Gadea, F. Nowacki, C. Andreoiu *et al.*, Observation of a core-excited  $E4$  isomer in  $^{98}\text{Cd}$ , *Phys. Rev. C* **69**, 064304 (2004).
- [37] N. Boelaert, N. Smirnova, K. Heyde, and J. Jolie, Shell model description of the low-lying states of the neutron deficient Cd isotopes, *Phys. Rev. C* **75**, 014316 (2007).
- [38] R. M. Clark, J. N. Wilson, D. Appelbe, M. P. Carpenter, C. J. Chiara, M. Cromaz, M. A. Deleplanque, M. Devlin, R. M. Diamond, P. Fallon *et al.*, Yrast and near-yrast excitations up to high spin in  $^{100}\text{Cd}_{52}$ , *Phys. Rev. C* **61**, 044311 (2000).
- [39] B. Maheshwari, H. Abu Kassim, N. Yusof, and A. K. Jain, Evolution of nuclear structure in and around  $Z=50$  closed shell: Generalized seniority in Cd, Sn and Te isotopes, *Nucl. Phys. A* **992**, 121619 (2019).
- [40] W. G. Jiang *et al.*, Accurate bulk properties of nuclei from  $a = 2$  to  $\infty$  from potentials with  $\Delta$  isobars, *Phys. Rev. C* **102**, 054301 (2020).
- [41] N. Shimizu, T. Mizusaki, Y. Utsuno and Y. Tsunoda, Thick-restart block Lanczos method for large-scale shell-model calculations, *Comput. Phys. Comm.* **244**, 372 (2019).
- [42] Z. H. Sun, G. Hagen, G. R. Jansen, and T. Papenbrock, Effective shell-model interaction for nuclei “southeast” of  $^{100}\text{Sn}$ , *Phys. Rev. C* **104**, 064310 (2021).
- [43] R. Machleidt, and H. Mütter, Charge symmetry breaking of the nucleon-nucleon interaction:  $\rho - \omega$  mixing versus nucleon mass splitting, *Phys. Rev. C* **63**, 034005 (2001).
- [44] A. Holt, T. Engeland, M. Hjorth-Jensen, and E. Osnes, Application of realistic effective interactions to the structure of the Zr isotopes, *Phys. Rev. C* **61**, 064318 (2000).
- [45] N. A. Smirnova, A. De Maesschalck, A. Van Dyck, and K. Heyde, Shell-model description of monopole shift in neutron-rich Cu, *Phys. Rev. C* **69**, 044306 (2004).
- [46] P.C. Srivastava, and I. Mehrotra, Monopole shift in odd neutron-rich F isotopes: A shell-model description, *Int. J. Mod. Phys. E* **20** (3) (2011) 637.
- [47] T. Otsuka *et al.*, Evolution of shell structure in exotic nuclei, *Rev. Mod. Phys.* **92**, 015002 (2020).
- [48] Evaluated Nuclear Structure Data File (ENSDF) <http://www.nndc.bnl.gov/ensdf/>.
- [49] M. Górska *et al.*,  $^{98}\text{Cd}_{50}$ : The Two-Proton-Hole Spectrum in  $^{100}\text{Sn}_{50}$ , *Phys. Rev. Lett.* **79**, 2415 (1997).
- [50] G. de Angelis *et al.*, Excited states in  $^{104}\text{Cd}$  described with the interacting boson model plus broken pairs, *Phys. Rev. C* **60**, 014313 (1999).
- [51] T. J. Gray *et al.*, E2 rotational invariants of  $0_1^+$  and  $2_1^+$  states for  $^{106}\text{Cd}$ : The emergence of collective rotation, *Phys. Lett. B* **834**, 137446 (2022).
- [52] A. Gade *et al.*, First observation of the intruder band in  $^{108}\text{Cd}$ , *Phys. Rev. C* **65**, 041305(R) (2002).
- [53] P. E. Garrett *et al.*, Quadrupole-octupole coupled states in  $^{112}\text{Cd}$ , *Phys. Rev. C* **59**, 2455 (1999).
- [54] A. Jungclaus *et al.*, High-spin states in the vibrational nucleus  $^{114}\text{Cd}$ , *Eur. Phys. J. A* **20**, 55 (2004).
- [55] Y. Wang *et al.*,  $\beta$  decay of neutron-rich  $^{118}\text{Ag}$  and  $^{120}\text{Ag}$  isotopes, *Phys. Rev. C* **67**, 064303 (2003).
- [56] M.A. Stoyer *et al.*, Spectroscopy of neutron-rich Pd and Cd isotopes near  $A=120$ , *Nuclear Physics A* **787**, 455 (2007)
- [57] A. Vancraeynest *et al.*, Prompt  $\gamma$ -ray spectroscopy of the neutron-rich  $^{124}\text{Cd}$ , *EPJ Web Conf.* **62**, 01004 (2013)
- [58] T. Kautzsch *et al.*, Structure of neutron-rich even-even  $^{124,126}\text{Cd}$ , *Eur. Phys. J. A* **25**, s01, 117 (2005).
- [59] A. Jungclaus *et al.*, Observation of Isomeric Decays in the  $r$ -Process Waiting-Point Nucleus  $^{130}\text{Cd}_{82}$ , *Phys. Rev. Lett.* **99**, 132501 (2007).
- [60] E. Caurier, G. Martínez-Pinedo, F. Nowacki, A. Poves, and A. P. Zuker, The shell model as a unified view of nuclear structure, *Rev. Mod. Phys.* **77**, 427 (2005).
- [61] B. Pritychenko, M. Birch, B. Singh, and M. Horoi, Tables of E2 transition probabilities from the first  $2^+$  states in even-even nuclei, *At. Data Nucl. Data Tables* **107** 1-139 (2016).

- [62] J. Park *et al.*, Properties of  $\gamma$ -decaying isomers and isomeric ratios in the  $^{100}\text{Sn}$  region, *Phys. Rev. C* **96**, 044311 (2017).
- [63] A. Ekström *et al.*, Electric quadrupole moments of the  $2_1^+$  states in  $^{100,102,104}\text{Cd}$ , *Phys. Rev. C* **80**, 054302 (2009).
- [64] Nuclear Electromagnetic Moments Compilation - IAEA NDS [www-nds.iaea.org/nuclearmoments/](http://www-nds.iaea.org/nuclearmoments/).
- [65] D. T. Yordanov *et al.*, Spins, Electromagnetic Moments, and Isomers of  $^{107-129}\text{Cd}$ , *Phys. Rev. Lett.* **110**, 192501 (2013).
- [66] X.F. Yang, S.J. Wang, S.G. Wilkins, and R.F. Garcia Ruiz, Laser Spectroscopy for the Study of Exotic Nuclei, [arXiv:2209.15228](https://arxiv.org/abs/2209.15228).
- [67] M. P. Fewell, R. H. Spear, G. K. Adam, and M. T. Esat, Determination of  $B(E3; 0_1^+ \rightarrow 3_1^-)$  Values for the Stable Isotopes of Cadmium, *Aust. J. Phys.* **38**, 555 (1985).
- [68] P.C. Srivastava, and L. Zamick, Minimal theory of isomerism- Q.Q and other interactions, *Phys. Scr.* **96**, 065307 (2021).
- [69] B. Bhoy, and P.C. Srivastava, Systematic shell model study for  $N = 82$  and  $N = 126$  isotones and nuclear isomers, *J. Phys. G: Nucl. Part. Phys.* **49** 085101 (2022).
- [70] B. Bhoy, and P.C. Srivastava, Systematic shell-model study of Rn isotopes with  $A = 207$  to  $216$  and isomeric states, *J. Phys. G: Nucl. Part. Phys.* **48** 125103 (2021).
- [71] Swati Garg, B. Maheshwari, B. Singh, Y. Sun, A. Goel, and A. K. Jain, Atlas of Nuclear Isomers - Second Edition, *Atomic Data and Nuclear Data Tables* **150**, 101546 (2023).
- [72] P. Axel, and M. Dancoff, Classification of Nuclear Isomers, *Phys. Rev.* **76**, 892 (1949).
- [73] K. Wimmer *et al.*, Isomeric states in neutron-rich nuclei near  $N = 40$ , *Phys. Rev. C* **104**, 014304 (2021).
- [74] J. Blachot *et al.*, Nuclear data sheets update for  $A = 104$ , *Nucl. Data Sheets* **64**, 1 (1991).
- [75] S.I. Sukhoruchkin *et al.*, Tables of Excitations of Proton- and Neutron-Rich Unstable Nuclei, *Springer-Verlag Berlin Heidelberg* 2008.
- [76] J. A. Pinston and J. Genevey, Microsecond isomers in the magic regions  $^{78}\text{Ni}$  and  $^{132}\text{Sn}$ , *J. Phys. G* **30**, R57 (2004).